The effect of climate change on the simulated streamflow of six Canadian rivers based on the CanRCM4 regional climate model

Vivek. K. Arora[1], Aranildo Lima[1], Rajesh Shrestha[2]

[1]Canadian Centre for Climate Modelling and Analysis, Climate Research Division, Environment Canada, Victoria, BC, Canada
[2]Climate Research Division, Environment and Climate Change Canada, Victoria, BC, Canada

Correspondence to: Vivek K. Arora (vivek.arora@ec.gc.ca)

Abstract

The effect of climate change on the hydro-climatology, in particular streamflow, of six major Canadian rivers (Mackenzie, Yukon, Columbia, Fraser, Nelson, and St. Lawrence) is investigated by analyzing results from the historical and future simulations (RCP 4.5 and 8.5 scenarios) performed with the Canadian regional climate model (CanRCM4). Streamflow is obtained by routing runoff using river networks at 0.5° resolution. Of these six rivers, Nelson and St. Lawrence are the most regulated. As a result, the streamflow at the mouth of these rivers shows very little seasonality. Additionally, the Great Lakes significantly dampen the seasonality of streamflow for the St. Lawrence River. Mean annual precipitation (P), evaporation (E), runoff (R), and temperature increase for all six river basins in both future scenarios considered here, and the increases are higher for the more fossil fuel-intensive RCP 8.5 scenario. The only exception is the Nelson River basin for which the simulated runoff increases are extremely small. The hydrological response of these rivers to climate warming is characterized by their existing climate states. The northerly Mackenzie and Yukon River basins show a decrease in evaporation ratio (E/P) and an increase in runoff ratio (R/P) since the increase in precipitation is more than enough to offset the increase in evaporation associated with increasing temperature. For the southerly Fraser and Columbia River basins, the E/P ratio increases despite an increase in precipitation, and the R/P ratio decreases due to an already milder climate in the Pacific north-western region. The seasonality of simulated monthly streamflow is also more affected for the southerly Fraser and Columbia Rivers than for the northerly Mackenzie and Yukon Rivers as snow amounts decrease and snowmelt occurs earlier. The streamflow seasonality for the Mackenzie and Yukon rivers is still dominated by snowmelt at the end of the century even in the RCP 8.5 scenario. The simulated streamflow regime for the Fraser and Columbia Rivers shifts from a snow-dominated to a hybrid/rainfall-dominated regime towards the end of this century in the RCP 8.5 scenario. While we expect the climate change signal from CanRCM4 to be higher than other climate models, owing to the higher-than-average climate sensitivity of its parent global climate model, the results presented here provide a consistent overview of hydrological changes across six major Canadian river basins in response to a warmer climate.

1. Introduction

As the global population and the standard of living increases so does the strain on freshwater resources. The natural availability of water is determined by the balance between precipitation (P) and evaporation (E) (this includes both evaporation and transpiration from plants). When precipitation exceeds evaporation, which is determined primarily by available energy, the water that does not evaporate or transpire (either at the surface or after infiltration into the soil) termed runoff (R) is carried by the rivers to the oceans. The seasonality of precipitation, its partitioning into snow and rainfall, and the seasonality of snowmelt and evaporation, all of which are determined by the climate in a given catchment or river basin eventually determine the seasonality of runoff. As anthropogenic climate change progresses, changes in the mean annual amounts and the seasonality of these different water budget components will lead to corresponding changes in runoff (Trenberth et al., 2007). Changes in precipitation extremes are also expected to lead to corresponding changes in the extremes of streamflow. The changes in streamflow have implications for floods and power generation. While runoff is expressed in similar units to precipitation and evaporation (depth of water per unit time, e.g. mm/s or m/year), streamflow is the volume of water generated per unit time (e.g. m^3/s or km^3/year) and requires multiplication with the area over which runoff is generated. Streamflow is also routed down the river network which introduces a time lag and attenuation of the peak runoff.

Output from climate and Earth system models (ESMs) remains the primary source of information for evaluating climate change impacts. Current approaches that rely on information generated by ESMs, to obtain an estimate of how future streamflow may potentially change, may

be classified into two broad categories. The first approach uses simulated runoff directly from the land surface component of single or multiple climate models which may be routed downstream to obtain streamflow at the mouths of river basins and at different points along a given river network (Arora and Boer, 2001; Miller and Russell, 1992; Zhang et al., 2014). Using direct runoff output from climate models has the benefit that the calculated changes in runoff are physically consistent with the altered radiative balance of the Earth in response to increases in the concentrations of greenhouse gases (GHGs). The corresponding changes in the general circulation of the atmosphere result in the associated changes in near-surface temperature, precipitation, and the hydrological cycle. However, this approach suffers from three limitations – 1) the biases in the climate simulated by the climate model, 2) the fact that the land surface components of climate models are not calibrated for a given river basin but rather designed to operate in a reasonably realistic way over the whole globe, and 3) the coarse resolution of global climate models (GCMs). The last limitation is partially addressed when data from finer-resolution regional climate models is used. The biases in the simulated climate do affect the simulated runoff for the current climate. Despite this, the approach can effectively capture the effects of climate change including increased evaporative demand (Winter and Eltahir, 2012), reduced snowpack (Salathé et al., 2010; Shrestha et al., 2021a), increased winter streamflow, and earlier snowmelt-driven peak flow (L. Sushama et al., 2006; Poitras et al., 2011). The second approach attempts to overcome these limitations by downscaling and/or bias-correcting climate from climate models for future scenarios and uses that to drive a well-calibrated hydrological model for given catchments or river basins (Gosling et al., 2011; Ismail et al., 2020; Miller et al., 2021; Yoosefdoost et al., 2022). The second approach is more prevalent for watershed to regional scale

impacts and adaptation studies. Given the large effort involved in downscaling and bias-correcting raw climate data from climate models, most current impact studies use downscaled and bias-corrected data put together by other groups rather than specifically doing this for their project. Recent examples include the downscaled and bias-corrected climate data for the conterminous United States (Thrasher et al., 2013) based on climate model output from the fifth phase of the Coupled Model Intercomparison Project (CMIP5), and statistically downscaled and bias-corrected data from five CMIP5 models, available at the global scale, tailored to the requirements of the Inter-Sectoral Impact Model Intercomparison Project (ISIMIP) (Lange, 2019). Both these data sets have found large applications in the impacts and adaptation community. The processes of downscaling and bias correction are distinct, and they both have their inherent limitations. There are several examples of the limited ability of bias-correction to correct and downscale variability, and that bias-correction can potentially cause implausible climate change signals (Maraun, 2016; Maraun et al., 2017). There are also uncertainties, substantial contradictions, and sensitivity to assumptions between the different downscaling methods (Hewitson et al., 2014).

Finally, while land surface models are typically used within the coupled framework of climate models, hydrological models are typically used as a standalone model for impact studies. While the primary output quantities from hydrological models are runoff and streamflow, land surface models output a range of water, energy, and CO_2 fluxes. The layer of air directly above the land surface, commonly referred to as the atmospheric or planetary boundary layer, is affected by surface-atmosphere exchanges of energy and water and extends upward into the atmosphere. A realistic representation of turbulent fluxes of energy and water in the planetary

boundary layer is essential to the transport of moisture and energy through the atmosphere. As a result, while calibration of hydrological models to reproduce observed streamflow is a routine exercise (Chegwidden et al., 2019; Hattermann et al., 2018; Huang et al., 2020; Hundecha et al., 2020), land surface models cannot be calibrated to reproduce a single or a small subset of quantities. Rather land surface models are expected to reproduce reasonably realistic estimates of a range of energy, water, and CO_2 fluxes over the whole globe. The philosophy behind land surface models, as they are used in the context of climate models, is that given 1) a model's structure and parameterizations, 2) the driving geophysical data for fields such as vegetation cover, soil depth, and soil texture, and 3) the driving meteorological variables, a model is expected to reasonably realistically reproduce various components of the water, energy, and carbon cycle at the global scale. The global scale of land surface models within the framework of climate models precludes tuning of their parameters for individual grid cells or for a region (e.g. a river basin) to reproduce a small subset of model outputs.

While well-calibrated hydrological models are generally suitable for a given catchment or a river basin their application cannot be easily extended to large-scale global or regional hydrologic modelling studies since it is typically not feasible to tune model parameters for all grid cells in a large domain. For a large region like Canada correctly representing anthropogenic regulation, using downscaled and bias-corrected climate data from an ensemble of climate models is a challenging task, and that is why it has only been done for a selected few river basins in Canada, and that too considering one river basin at a time. In the end, both approaches have their strengths and limitations for assessing climate change impacts on hydrology and can be considered complementary to each other.

Future hydrologic projections using the second approach (hydrological modes driven by statistically downscaled and bias-adjusted climate models) are available for selected river basins in Canada. The results over the Prairies and British Columbia (Shrestha et al., 2021b; Sobie and Murdock, 2022) generally indicate shorter snow cover duration, earlier snowmelt, and reduced annual maximum snow water equivalent as the climate warms. Streamflow projections across Canada generally indicate earlier snowmelt-driven peak flow, increased winter flow, and decreased summer flow (Budhathoki et al., 2022; Dibike et al., 2021; Islam et al., 2019; MacDonald et al., 2018; Shrestha et al., 2019). Annual streamflow is projected to increase, with higher increases in the northern basins (Bonsal et al., 2020; Stadnyk et al., 2021). However, these projections are based on different climate and hydrological models, downscaling methods, emissions scenarios, and future periods, and no consistent set of projections is available across all major river basins of Canada.

In this study, we have used the first approach to provide a consistent set of projections across all major river basins of Canada, while being cognizant of its limitations. We investigate the effect of climate change on the annual, monthly, and daily streamflow characteristics of six major Canadian rivers (Mackenzie, Yukon, Columbia, Fraser, Nelson, and St. Lawrence) using runoff output from simulations performed with version 4 of the Canadian Regional Climate Model (CanRCM4) (Scinocca et al. 2016). The river basins of the Yukon and Columbia Rivers cover part of the United States of America as well. We used daily runoff generated from CanRCM4 for the historical period and for the two future scenarios (representative concentration pathways (RCP) 4.5 and 8.5). The spatial resolution of runoff data from CanRCM4 is 0.22° which is equivalent to about 12 km at 60° N (Canada lies between approximately 42°N and 83°N). We

then routed this runoff through river networks at 0.5° resolution to evaluate streamflow at the mouths of major Canadian rivers. The Mackenzie, Yukon, and Fraser Rivers are somewhat less regulated than the heavily regulated Nelson, Columbia, and St. Lawrence Rivers. The routing scheme used here does not take into account dams and reservoirs and therefore the modelled streamflow represents natural streamflow. This aspect is discussed in more detail in Section 2.

2. Models and data

Equation (1) summarizes the water balance over a given grid cell or a river basin for a given timescale.

$$P = E + R + \Delta S \quad (1)$$

where ΔS is the change in water storage including that in soil moisture, snow, and the canopy water storage. All terms are expressed in depth per unit time units (e.g. mm/year). When a system is in equilibrium, at annual or longer timescales $\Delta S = 0$ and $P = E + R$. ΔS, however, may not be zero even over long timescales when a system is not in equilibrium e.g., when snow is accumulating or is melting consistently. We evaluated the P, E, and R components of equation (1) simulated by CanRCM4 for each of the six river basins, considered in this analysis, and routed R to obtain streamflow at the river mouths.

2.1 The Canadian Regional Climate Model (CanRCM4)

CanRCM4 uses the fourth-generation Canadian atmospheric physics (CanAM4) package (von Salzen et al., 2013), which is the product of a multi-decadal program of climate model development at the Canadian Centre for Climate Modelling and Analysis (CCCma), a section

within Environment and Climate Change Canada. The CanAM4 atmospheric physics package is also used in CanESM2 (Arora et al., 2011) which contributed results to CMIP5. The difference between CanRCM4 and CanESM2, other than the former being a regional climate model and the latter being a comprehensive global ESM, is that CanRCM4 employs the limited-area configuration of the Global Environmental Multiscale (GEM) model (Côté et al., 1998), which uses a semi-Lagrangian dynamical core for advection in the atmosphere and is developed by Environment and Climate Change Canada's Recherche en Prévision Numérique (RPN) where it is used both for global and regional numerical weather prediction. CanESM2 on the other hand uses a spectral dynamical core for advection in the atmosphere. CanRCM4 is driven at its boundaries with data from its parent model (CanESM2). An overview and technical details of the coordinated global and regional climate modelling effort used to develop the CanESM2-CanRCM4 system are described in detail by Scinocca et al. (2016). Results from the model's North American 0.22° domain, for a single ensemble member, are primarily used here. In addition, we also used runoff from CanRCM4 0.44° resolution simulations for the North American domain because of the availability of a large ensemble (LE) of 50 members (CanRCM4 LE) (ECCC, 2018). The large ensemble simulations allow the consideration of CanRCM4's internal variability, which is an intrinsic property of the climate system and models, that is largely irreducible and could account for a large fraction of the inter-climate model spread (Deser et al., 2020). The results used here from CanRCM4 form part of its contribution to the coordinated regional climate downscaling experiment (CORDEX) effort. The North American domain of CanRCM uses a rotated latitude-longitude projection with the North Pole at longitude 83° E and latitude 42.5° N, as opposed to the geographic North Pole (longitude 0°E, latitude 90° N).

The land surface component in CanAM4 is the coupled CLASS-CTEM model. The physical processes are based on the Canadian Land Surface Scheme (CLASS) (Verseghy, 1991; Verseghy et al., 1993), and biogeochemical processes (which simulate vegetation as a dynamic component of the climate system) are based on the Canadian Terrestrial Ecosystem Model (CTEM) (Arora and Boer, 2003, 2005). The configuration of CLASS-CTEM used in CanESM2 and CanRCM4 uses three soil layers with thicknesses of 0.10, 0.25, and 3.75 m. Liquid and frozen soil moisture contents, and soil temperature, are determined prognostically for the three soil layers. The temperature, albedo, mass, and density of a single-layer snow pack (when environmental conditions permit snow to exist) are also prognostically modelled. Surface runoff is generated in CLASS when precipitation intensity exceeds infiltration capacity and when the top soil layer is saturated. The rainwater and snow melt that infiltrate the soil are available for soil evaporation and transpiration. Any remaining water percolates down the soil profile and comes out at the bottom of the soil profile and is termed drainage. Combined surface runoff and drainage constitute total runoff. Like most land surface components of ESMs, CLASS does not include a groundwater representation. Surface runoff and drainage from CLASS are used as input into a large-scale river routing scheme to route runoff and obtain streamflow at the mouth of the rivers considered in this study as explained in the next section.

2.2 Variable velocity routing model

The variable velocity river routing scheme of Arora and Boer (1999) that is implemented in the family of Canadian ESMs (CanESMs) (Arora et al., 2009, 2011; Swart et al., 2019) is used to route daily runoff from CanRCM4. This routing scheme has been implemented in various versions of CanESMs at a spatial resolution of 2.81° since the year 2000. For this study, the routing scheme

was implemented at a spatial resolution of 0.5°. The reason for using river routing at 0.5° resolution instead of scaling river networks to the 0.22° rotated latitude-longitude projection of CanRCM4 's North American domain is that scaling river networks is a non-trivial and cumbersome task that cannot be fully automated (Arora and Harrison, 2007). In contrast, conservatively regridding runoff from one spatial resolution to another is a straightforward process. In addition, it has been shown that routing is not very sensitive to the spatial scale at which it is performed. Specifically, Arora et al. (2001) evaluated the Arora and Boer (1999) routing scheme together with the WATROUTE routing scheme at ~350 km and ~25 km spatial resolutions, respectively, for the Mackenzie River basin. The two routing schemes were driven with the same runoff. Arora et al. (2001) conclude that for the purpose of realistically modelling streamflow at the mouth of the rivers in climate models, flow routing at large spatial scales gives similar results to routing at finer spatial scales. In our study, the difference between the spatial resolution of runoff (0.22° and 0.44°) from the CanRCM4 model and routing (0.5°) is much smaller than the Arora et al. (2001) study. As a result, we do not expect that routing at a slightly different spatial resolution than runoff will lead to significant differences in the simulated streamflow. The routing scheme needs river flow directions and these are obtained from the Total Integrating Runoff Pathways (TRIP) data set (http://hydro.iis.u-tokyo.ac.jp/~taikan/TRIPDATA/TRIPDATA.html, last accessed July 2023) of Oki and Sud (1998). The TRIP data are available at the regular latitude-longitude grid with the geographic North Pole at its usual location (0° E, 90° N). Figure 1 shows the river networks at 0.5° resolution based on TRIP data which also identifies the six river basins investigated in this study. The Fraser River (identified by the light green colour) appears to have a river mouth over land. This is because the Fraser River drains into the narrow Strait of Georgia

which is not resolved at the 0.5° resolution of the TRIP data set. In addition, the TRIP data set does not resolve any inland lakes and provides river flow directions over grid cells that are lakes. This is in fact helpful because it avoids discontinuities in the river network.

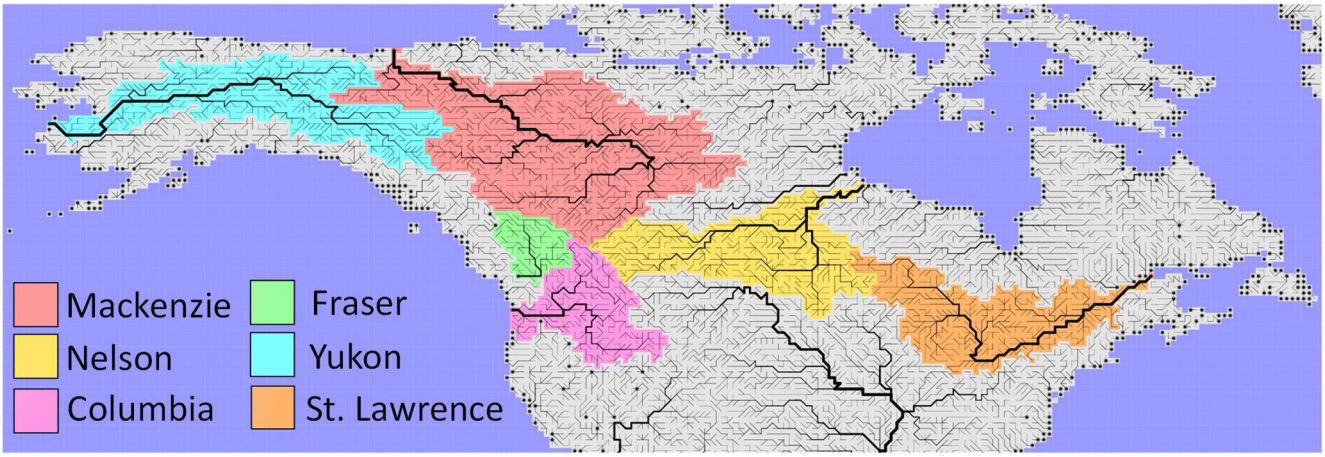

Figure 1: River flow networks at 0.5° resolution used in this study. The major river basins for which streamflow and runoff are analyzed in this study are also identified.

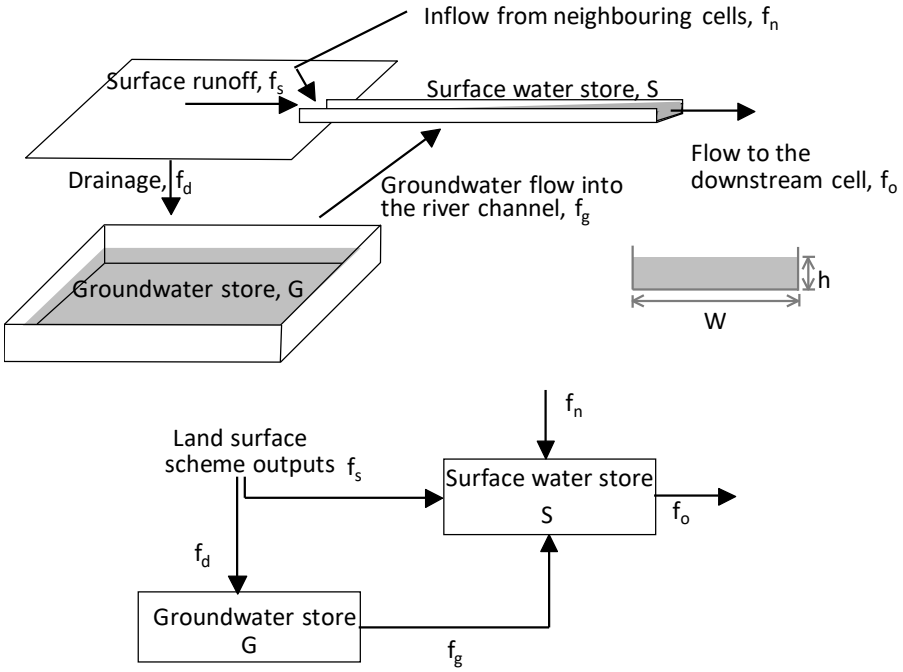

Figure 2: Schematic of the Arora and Boer (1999) river routing scheme used in this study to route runoff simulated by CanRCM4.

240

241 Figure 2 shows the schematic of the routing scheme which uses surface runoff and
242 drainage outputs from the land surface scheme. The variable velocity routing scheme used here
243 is described briefly below and more details can be found in Arora and Boer (1999). The water
244 balance within a grid cell for its surface S (m^3) and groundwater G (m^3) stores is given by

245 $$\frac{dS}{dt} = f_s + f_n + f_g - f_o \quad (2)$$

246 $$\frac{dG}{dt} = f_d - f_g \quad (3)$$

247 where, f_s and f_d are the surface runoff and drainage (or baseflow) estimates given by the land
248 surface scheme, f_n and f_o are the surface water inflow from the adjacent upstream neighbouring
249 grid cell(s) and outflow to the downstream grid cell respectively, and f_g is the groundwater
250 outflow from the groundwater reservoir to the surface water reservoir within a grid cell as shown
251 in Figure 2. The fluxes are represented in m^3/s.

252 A river channel is assumed to be rectangular and the width (W) of the river at every point
253 along the river network is specified a priori. This river width in meters is calculated based on its
254 geomorphological relationship with mean annual discharge. The surface runoff contributes
255 directly to the surface water store which is essentially the amount of water in the rectangular
256 river channel between two grid cells. The flow velocity (V, m/s) is calculated using the Mannings
257 formula (Manning, 1891).

258 $$V = \frac{1}{r} R^{2/3} S^{1/2} = \frac{1}{r} \left(\frac{A}{P}\right)^{2/3} n^{1/2} = \frac{1}{r} \left(\frac{Wh}{W+2h}\right)^{2/3} n^{1/2} \quad (4)$$

where *r* is the unitless Mannings roughness coefficient (a default value of 0.04 is used), *A* is the area of the river channel (m^2), *P* is the wetted perimeter (m), and *h* is the depth of water in the channel (m). The slope *n* (unitless) of the channel is calculated using elevation difference and the river length between two grid cells.

The river channel storage S is assumed to be a linear function of outflow discharge, so

$$S = \tau f_o = \frac{L}{V} AV = LA = LWh \tag{5}$$

where τ is the travel time between the grid cell under consideration and its downstream neighbor given by $\tau = L/V$, where *L* is the distance between the grid cells (m). The outflow f_o is given by

$$f_o = AV = WhV = Wh\frac{1}{r}\left(\frac{Wh}{W+2h}\right)^{2/3} n^{1/2} \tag{6}$$

and substituting (5) and (6) into (2) yields

$$\frac{dh}{dt} = \frac{1}{LW}\left(I - \frac{W^{5/3}h^{5/3}}{r(W+2h)^{2/3}}\, n^{1/2}\right)^{\square} \tag{7}$$

where *I* (m^3/s) is the total inflow into a grid cell ($I = f_s + f_n + f_g$). Equation (7) describes the flow in terms of the rate of change of flow depth for a given river section. An explicit forward step finite difference approximation for (7) yields

$$h(t+1) = h(t) + \frac{\Delta t}{LW}\left(I(t) - \frac{W^{5/3}h(t)^{5/3}}{r(W+2h(t))^{2/3}}\, n^{1/2}\right)^{\square} \tag{8}$$

Flow velocity and outflow discharge for the river channel at any time step can be obtained using equations (4) and (6). For the 0.5° resolution used here, a stable solution of (8) is obtained with

277 Δt equal to around 10 minutes. The approach yields dynamically-varying flow depth, velocity,
278 and discharge through the river channel in response to changing surface and baseflow runoff
279 inputs from the land surface model.

280 The groundwater component of the routing model assumes that groundwater storage, *G*,
281 is a linear function of groundwater outflow, f_g.

282 $$G = \tau_g \, f_g \tag{9}$$

283 The delay in groundwater storage (τ_g) is based on the dominant soil texture type and is set to 10,
284 35, and 65 days if the dominant soil type in each grid cell is sand, silt, and clay, respectively,
285 following Arora and Boer (1999). Substituting G in equation (3) yields

286 $$\tau_g \frac{df_g}{dt} = f_d - f_g \tag{10}$$

287 and following Arora and Boer (1999) we use the following expression

288 $$f_g(t+1) = f_g(t)\, e^{-\Delta t/\tau_g} + \left(1 - e^{-\frac{\Delta t}{\tau_g}}\right) f_d(t) \tag{11}$$

289 to determine discharge from the groundwater reservoir within a grid cell and to step forward in
290 time, where a time step Δt equal to three hours is used. The simplistic form of equation (11)
291 allows to use a much larger time step than the time step of 10 minutes required for equation (8).

292 The routing scheme used here does not consider the flow regulation effect of dams and
293 reservoirs. It, however, does consider the effect of lakes and ice jams in a simple manner. The
294 global lake data set from Kourzeneva et al. (2012) is used which prescribes the fractional coverage
295 of sub-grid lakes and the five Laurentian Great Lakes (Lakes Superior, Michigan, Huron, Ontario,

and Erie). In particular, the flow at the mouth of the St. Lawrence River is affected significantly by the Great Lakes. The hydraulic residence time of water in the Great Lakes varies from about 2 years for Lake Erie to about 200 years for Lake Superior (Quinn, 1992). As a result, even in the absence of anthropogenic flow regulation for the St. Lawrence River, we expect the streamflow at its mouth to show very little seasonality compared to the usual spring peak of Canadian rivers dominated by snowmelt. The simple approach used here delays the streamflow flowing into a grid cell with a lake fraction greater than 60% using an e-folding time scale of 300 days similar to the treatment of the groundwater reservoir (Figure 2) (Arora and Boer, 1999). For the St. Lawrence River, the effect of delay caused by the Great Lakes is much larger than that of the anthropogenic flow regulation.

Ice jams and breakups are complex thermal and mechanical events and therefore challenging to model. They occur on all Canadian rivers with varying degrees and depend on winter temperatures, the river bathymetry, and the physical and geomorphological conditions of rivers (Beltaos, 2000; Prowse, 1986). The winter freezing of river water inevitably leads to a slow down of river flow velocity. When water cannot move downstream, upstream flooding results. Here, we have used a simple approach that increases Manning's roughness coefficient for the Mackenzie and the Yukon Rivers (which are the most northerly and therefore affected the most by ice jams) for the period January to June. The value of Manning's roughness coefficient is increased linearly from 0.04 to 0.08 from 1 January to 31 January, kept at 0.08 from 1 Feb to 31 May, and then reduced linearly from 0.08 to 0.04 over the period June 1 to 30 June. Chen and She (2020) report the trend in river ice breakup dates for the Mackenzie and Yukon Rivers to be around -0.3 and -1.3 days/decade for the 1950-2016 period, where the negative sign indicates

318 that the ice breakup is occurring earlier. Assuming the same trend, the breakup dates would
319 occur about 2.5 and 11 days earlier towards the end of this century, respectively, for the
320 Mackenzie and Yukon rivers. This simple approach reduces the river flow velocity during the
321 months that are most affected by river ice jams. Although this is not a perfect nor a complete
322 approach this simple treatment allows to improve the streamflow seasonality for the Mackenzie
323 and Yukon rivers. For the southerly Fraser and Columbia rivers such treatment was not necessary.
324 Consideration of a higher roughness coefficient for the St. Lawrence River to account for ice jams
325 does not affect its streamflow's seasonality (or rather the lack of it) which is overwhelmingly
326 determined by the delay and storage caused by the Great Lakes.

327 **2.3 Modelled and observation-based data**

328 The CMIP5 historical simulation covers the period 1850-2005 and the future scenarios
329 cover the period 2006-2100. We used daily runoff from CanRCM4 from its 0.22° North American
330 domain for the 20 years 1986-2005 from one ensemble member of the historical simulation and
331 for the 20 years 2081-2100 from one ensemble member each for the two future scenarios (RCP
332 4.5 and RCP 8.5, Moss et al. (2010)). The RCP 8.5 is the highest baseline emissions scenario where
333 future development is based on continuous fossil-fuel development. As a result, CO_2 emissions
334 and concentrations increase throughout the 21st century and CO_2 concentration in the year 2100
335 is around 1100 ppm. RCP 4.5 is a moderate emissions scenario in which emissions peak around
336 2040 and then decline: as a result CO_2 somewhat stabilizes to around 550 ppm by the year 2100.
337 Since the CanRCM4 data are available on a rotated latitude-longitude grid and the river routing
338 is performed on a regular latitude-longitude grid (following the TRIP data), the runoff data from
339 CanRCM4 are conservatively regridded to the global 0.5° grid using climate data operators (CDO)

(https://code.mpimet.mpg.de/projects/cdo/embedded/index.html#x1-7170002.12.5, last accessed Dec 2023) as mentioned earlier. These runoff data are then used as input into the routing model. The 20-year runoff data (1986-2005 for the historical simulation, and 2081-2100 for the future scenarios) are concatenated into a 40-year time series for each simulation (historical, RCP 4.5, and RCP 8.5). These data are then input into the routing model and the last 20 years of simulated streamflow are analyzed. The 20-year spin-up is sufficient to allow the surface and groundwater stores to fill up and reach equilibrium. The simulated precipitation and temperature from CanRCM4 are compared against observation-based data from the CRU TS 4.07 product (Harris et al., 2020).

The simulated streamflow is compared against observation-based estimates obtained from the Global Runoff Data Centre (GRDC) for the stations that are closest to the river mouths. Table 1 lists the drainage areas of all rivers considered in this study as discretized in the TRIP data set and at the stations closest to the river mouth. For the Columbia River, which is heavily regulated, we obtain an estimate of the naturalized flow with no regulation and no irrigation provided by the Bonville Power Administration (BPA) for the station VAN (near Vancouver, Washington, USA) (https://www.bpa.gov/energy-and-services/power/historical-streamflow-data;https://www.bpa.gov/-/media/Aep/power/historical-streamflow-reports/historic-streamflow-nrni-flows-1929-2008-corrected-04-2017.csv, last accessed July 2023). The drainage area of the Columbia River upstream of the VAN station is 616960 km^2 and does not include discharge contributions from three tributaries (Willamette, Cowlitz, and Lewis Rivers). Of these three tributaries, the contribution from Willamette is the largest. We obtained naturalized streamflow for the Willamette River at the station SVN (drainage area 25,600 km^2) also from

BPA's website (https://www.bpa.gov/-/media/Aep/power/historical-streamflow-reports/correction-20220801.zip, from the file SVN6ARF_daily_COR.xlsx) and added it to the naturalized streamflow at the station VAN. This yields naturalized streamflow for the entire Columbia River basin, except the smaller Cowlitz, and Lewis Rivers, and represents a drainage area of 642,560 km^2 (see Table 1).

The Nelson River is affected by two large lakes, Lake Winnipeg and Lake Manitoba, and it is also heavily regulated. It currently has five dams towards the end of its journey as it flows into Hudson Bay. There are no upstream gauging stations close to the first upstream dam. In addition, water is also diverted from Churchill to the Nelson River. We were unable to obtain naturalized flow for the Nelson River from the Manitoba hydroelectricity company. Due to anthropogenic flow regulation on the Nelson River, the present-day streamflow shows very little seasonality (as shown later). As a result, we do not evaluate the simulated daily or monthly streamflow for the Nelson River and focus only on its mean annual value.

Table 1: Comparison of river basin areas as represented in the TRIP data and at the gauging station closest to the river mouth for the river basins considered in this study as obtained from the GRDC.

River basin	River basin area (million km^2)		Gauging station
	in the TRIP data set	at the gauging station closest to the river mouth	
Mackenzie	1.74	1.66	Arctic red river
Yukon	0.85	0.83	Pilot Station
Columbia	0.66	0.64	See section 2.3
Fraser	0.23	0.22	Hope
Nelson	1.07	1.06	Long Spruce generating station
St. Lawrence	1.11	0.77	Cornwall, Ontario

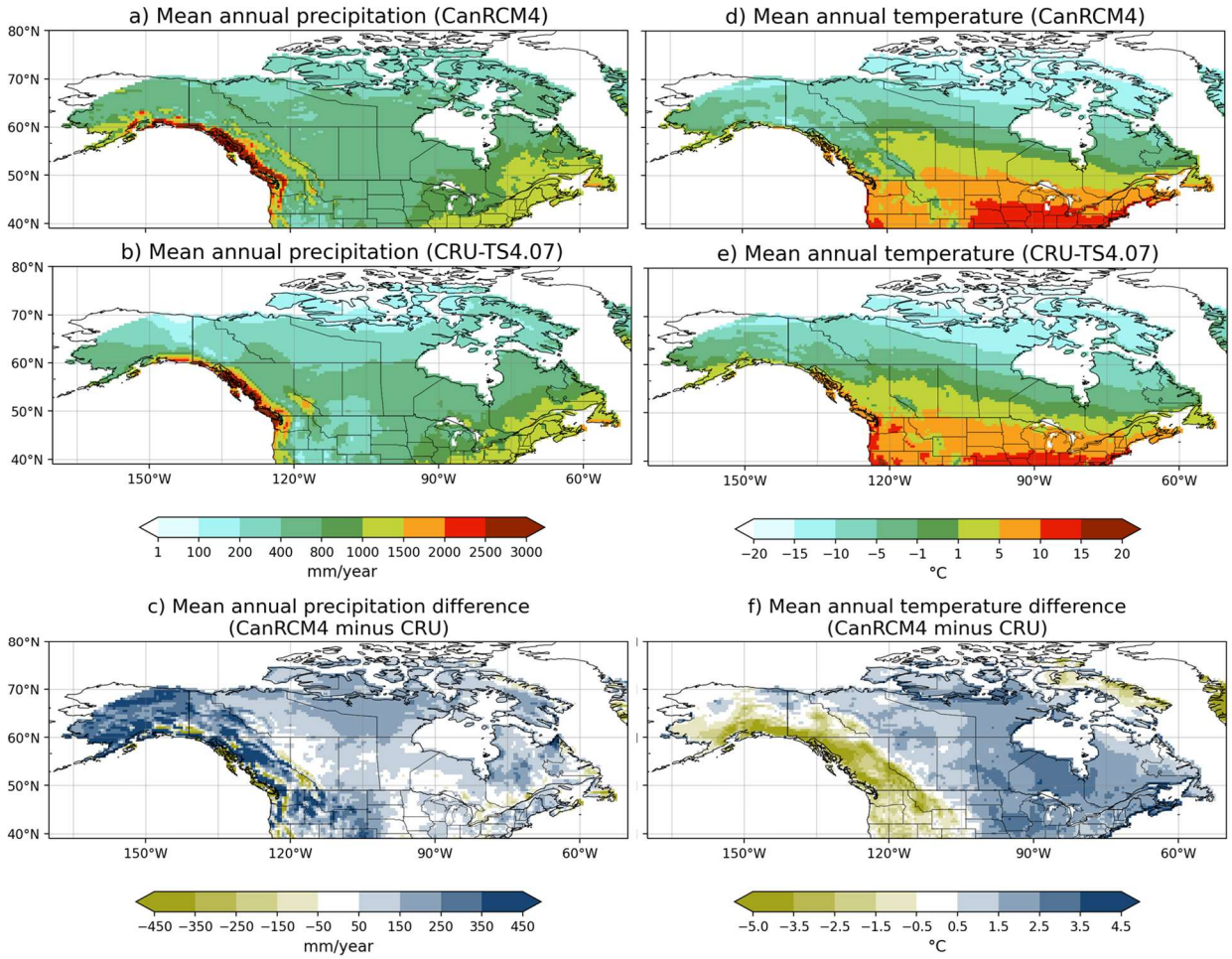

Figure 3: Comparison of CanRCM4 simulated precipitation (left column) and temperature (right column) with observation-based estimates from the CRU TS 4.07 data set for the period 1986-2005.

3. Results

3.1 Present-day precipitation, temperature, and streamflow

Figure 3 compares the geographical distribution of mean annual precipitation (left column) and temperature (right column) simulated by CanRCM4 to observation-based estimates from the CRU TS 4.07 data set (referred to as CRU from here on) for the 1986-2005 period. Although the six river basins considered in this study do not cover the entire Canadian region, for

completeness the plots are shown for the whole of Canada and south up to 39 °N to include the southern edge of the Columbia River basin. In Figure 3, while CanRCM4 broadly simulates the geographical distribution of temperature and precipitation reasonably realistically, there are differences compared to the CRU data set. CanRCM4 generally simulates higher precipitation over Canada and more so to the west of the Rockies (Figure 3c) compared to observations. The model simulates cooler than observed temperatures to the west of the Rockies and higher than observed temperatures to the east of the Rockies (Figure 3f). This is likely related to the representation of topography in the model. The overall somewhat higher precipitation in CanRCM4 over North America is also noted by Alaya et al. (2019) who compared probable maximum precipitation (PMP) calculated using CanRCM4 data to estimates based on several reanalyses. Alaya et al. (2019) concluded that among the three reanalyses they considered, CanRCM4 compared best with the National Centre for Environmental Prediction's (NCEP) Climate Forecast System Reanalysis.

Figure 4 compares the simulated annual cycle of temperature (left column) and precipitation (middle column) over the six river basins (Figure 1) selected in this study with observation-based estimates from CRU. The right-hand side column compares simulated streamflow for the six river basins with observation-based estimates from the GRDC. The basin-averaged values of temperature and precipitation are calculated by area weighting the values in the individual grid cells that lie inside a given river basin according to the TRIP data (Figure 1). The plots also show the mean annual values (dashed lines) on the plot and their magnitude in the legend. Figure 4 shows that overall CanRCM4 simulated basin-wide averaged temperatures compare reasonably well with observation-based estimates based on the CRU data for the

Mackenzie and the Yukon River basins. For the Columbia and Fraser, the simulated temperatures are lower for most months, and for the Nelson River basin, the CanRCM4 simulated temperatures are higher compared to the CRU data. The seasonal cycle of temperature compares well with the observation-based estimates from CRU data. Compared to temperature, there are larger differences in simulated CanRCM4 precipitation compared to the CRU data. Although CanRCM4 simulates the seasonality of precipitation reasonably well compared to the CRU data, simulated precipitation is higher for all river basins, consistent with Figure 3c. The comparison with the CRU data provides useful insights into simulated quantities. Specifically, despite the difference in the magnitudes, CanRCM4 provides a reasonable representation of the seasonality of precipitation, for example, higher winter precipitation in the southern Fraser and Columbia basins, and higher summer precipitation in the northern Mackenzie and Yukon basins. However, all observation-based data sets (including CRU) have their limitations. Wong et al. (2017) compared several gridded observation-based precipitation data sets over Canada and found that they all have limitations and the data sets compared best with gauge-based precipitation data in summer, followed by autumn, spring, and winter in order of decreasing quality. Sun et al. (2018) compare global precipitation from 22 gauge-, satellite-, and reanalysis-based products, including CRU, and quantify the uncertainty in the different precipitation estimates over timescales ranging from daily to annual. Shi et al. (2017) evaluated the CRU precipitation over large regions of China and found that CRU underestimates precipitation in that region compared to rain gauge records. Furthermore, observation-based precipitation datasets also generally tend to underrepresent total precipitation in mountainous western Canada (where the Yukon, Mackenzie, Fraser, and Columbia River basins are located) due to low station density at high elevations (Werner et al.,

436 2019). In the end, the objective of the comparison of the simulated climate with CRU
437 observations is to evaluate if the model climate is reasonably realistic for the present day. The
438 assumption behind using direct output from climate models is that despite the biases in the
439 simulated current climate it is possible to deduce meaningful information about the effect of
440 climate change using the change in simulated quantities.

441

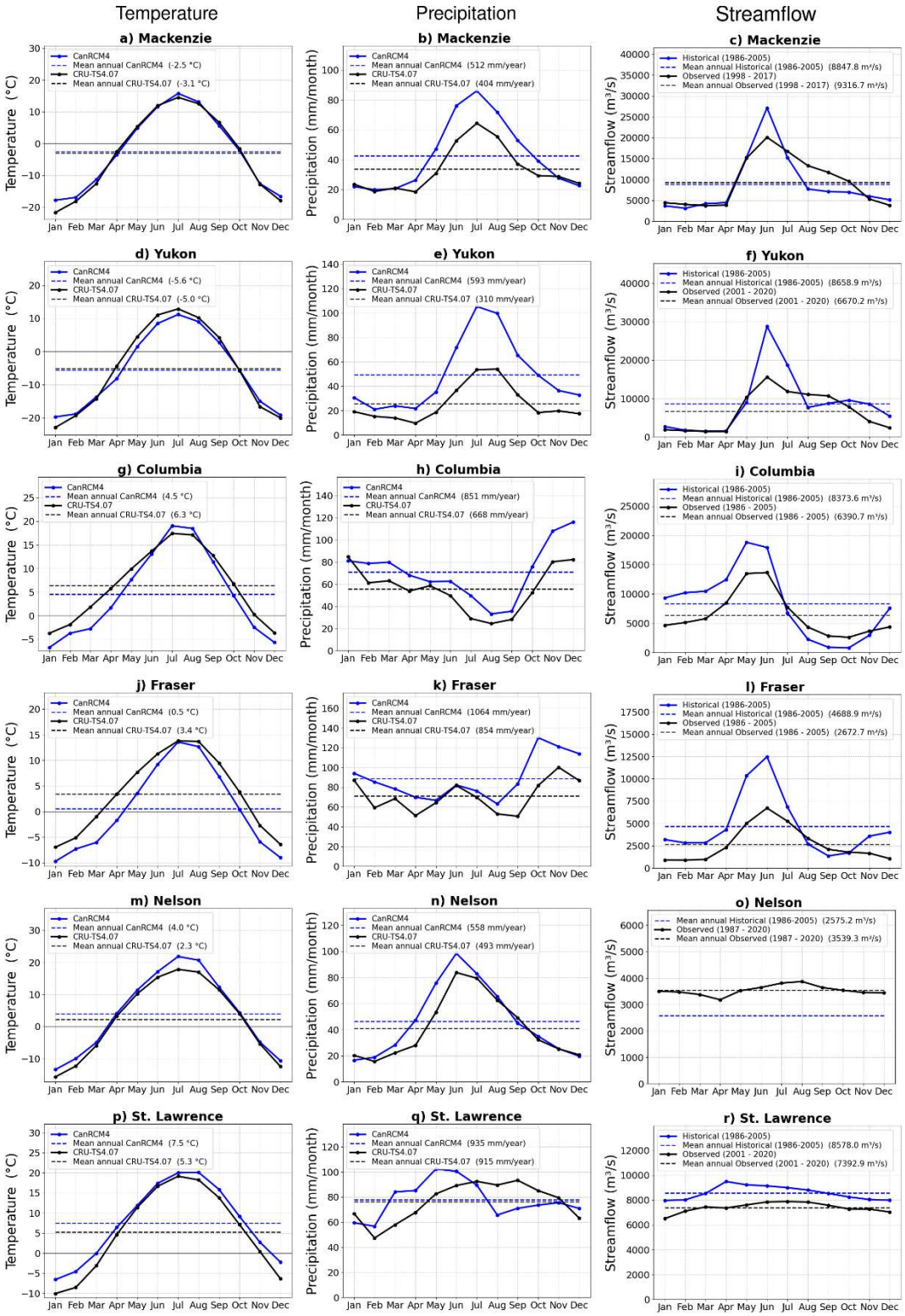

442

443 **Figure 4**: Comparison of the annual cycle of basin-wide averaged CanRCM4 simulated
444 temperature (left column) and precipitation (middle column) with observation-based estimates
445 from the CRU TS 4.07 data set for the period 1986-2005. The right-hand side column compares

simulated streamflow with observations from the GRDC. In the absence of the consideration of anthropogenic flow regulation for the Nelson River only its simulated mean annual streamflow value is evaluated.

The differences in simulated climate between CanRCM4 and the observation-based climate in CRU for the present day affect simulated streamflow as expected. The simulated mean annual streamflow is higher for four out of six river basins considered (Yukon, Columbia, Fraser, and St. Lawrence) primarily because of the higher simulated precipitation. Simulated precipitation is also higher for the Mackenzie River basin, but the mean annual simulated streamflow compares well with its observation-based estimate. Possible reasons for reasonably realistic annual simulated streamflow despite higher precipitation could be biases in the CRU data set itself (e.g., underrepresentation of total annual precipitation), or higher simulated evaporation in CanRCM4 (although simulated summer temperatures compare well with the CRU data). Finally, the simulated mean annual streamflow for the Nelson River is lower than its observation-based estimate despite somewhat higher simulated precipitation than the CRU data. The most likely reason for this is the diversion from the Churchill River into the Nelson River which started in 1976 to increase the water flow to larger generating stations on the lower Nelson River. The Manitoba government estimates that an average of 25% more water flows into the lower Nelson River due to the Churchill River Diversion (CRD) (https://www.gov.mb.ca/sd/water/water-power/churchill/index.html, last accessed Sep. 2023). The seasonality of streamflow for the Mackenzie, Yukon, and Fraser Rivers is dominated by the spring snowmelt with the peak occurring in June for both simulated and observed streamflow. The simulated streamflow for the Columbia and Fraser rivers peaks at the right time but there is more simulated streamflow during the winter months when precipitation is also higher than

observed. For the Mackenzie and Yukon rivers although the mean annual simulated and observed streamflow are comparable their seasonal distribution is not. The simulated streamflow peak for these rivers is higher due to the simple treatment of ice jams which is not sufficient to hold the water in the river channel and then release it slowly as ice jams slowly dissipate in the spring and summer months, as the observed streamflow indicates. Finally, for the St. Lawrence River, there is little seasonality in observed streamflow due to the delay caused by the Great Lakes and anthropogenic flow regulation. The lack of strong seasonality simulated in simulated streamflow for the St. Lawrence River is caused entirely due to the delay caused by the Great Lakes (section 2.2).

Overall the spatial distribution of precipitation and temperature over Canada (Figure 3), and the seasonality of these two primary climate drivers for the river basins considered in this study (Figure 4), compare reasonably well with observation-based estimates from the CRU data, although there are differences in the absolute magnitude of these variables. The resulting seasonality of streamflow has limitations due to three factors: 1) the biases in the driving climate from CanRCM4, 2) the biases in the land surface component of CanRCM4 which partitions precipitation into evaporation and runoff, 3) the lack of calibration of the land surface component to specific river basins, and 4) the lack of processes in the routing component including the limitation of not being able to treat ice jams comprehensively. Despite these limitations, the simulated streamflow captures the broad seasonal patterns with higher values during the spring snow melt and lower values during the winter months as observations show.

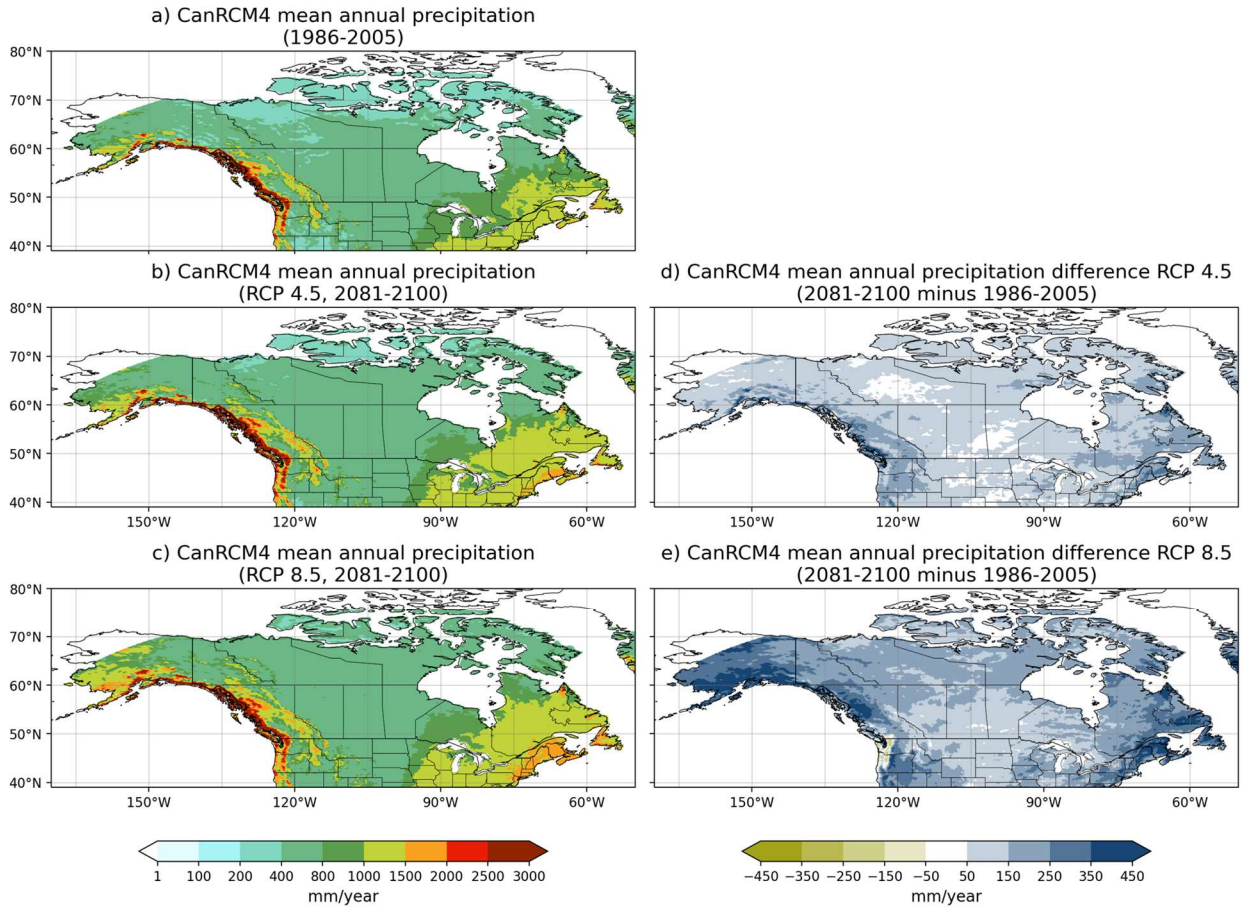

491 **Figure 5**: Comparison of CanRCM4 simulated precipitation for the 1986-2005 and for the 2081-
492 2100 periods for RCP 4.5 and 8.5 scenarios.
493

494 **3.2 Changes in future climate and streamflow**

495 Figures 5, 6, and 7 show the changes in CanRCM4 simulated precipitation, temperature,
496 and runoff for the period 2081-2100, for both RCP 4.5 and 8.5 scenarios, compared to the 1986-
497 2005 period from the historical simulation. Over Canada, simulated precipitation and
498 temperature increase almost everywhere and in both scenarios. As expected, the magnitude of
499 precipitation and temperature change is higher for the RCP 8.5 than the RCP 4.5 scenario.
500 Simulated precipitation increases are higher in the coastal western and eastern Canadian regions
501 than in central and northern parts of Canada. The central Canadian region sees the lowest

increase in precipitation in both scenarios. Simulated temperature increases, as expected, are higher at higher latitudes due to polar amplification of the temperature change associated with the snow- and ice-albedo feedbacks. In the RCP 4.5 and 8.5 scenarios, the simulated temperature changes vary from about 3 °C and 6 °C, respectively, in the south, to about 6 °C and 11 °C, in the north. The parent climate model (CanESM2) on which CanRCM4 is based has an equilibrium climate sensitivity of 3.7 °C, somewhat on the higher side, compared to the range of 1.5 °C to 4.5 °C amongst climate models that contributed to CMIP5 (Schlund et al., 2020). As a result, we also expect the magnitude of simulated changes to be somewhat higher than a model with average climate sensitivity.

518

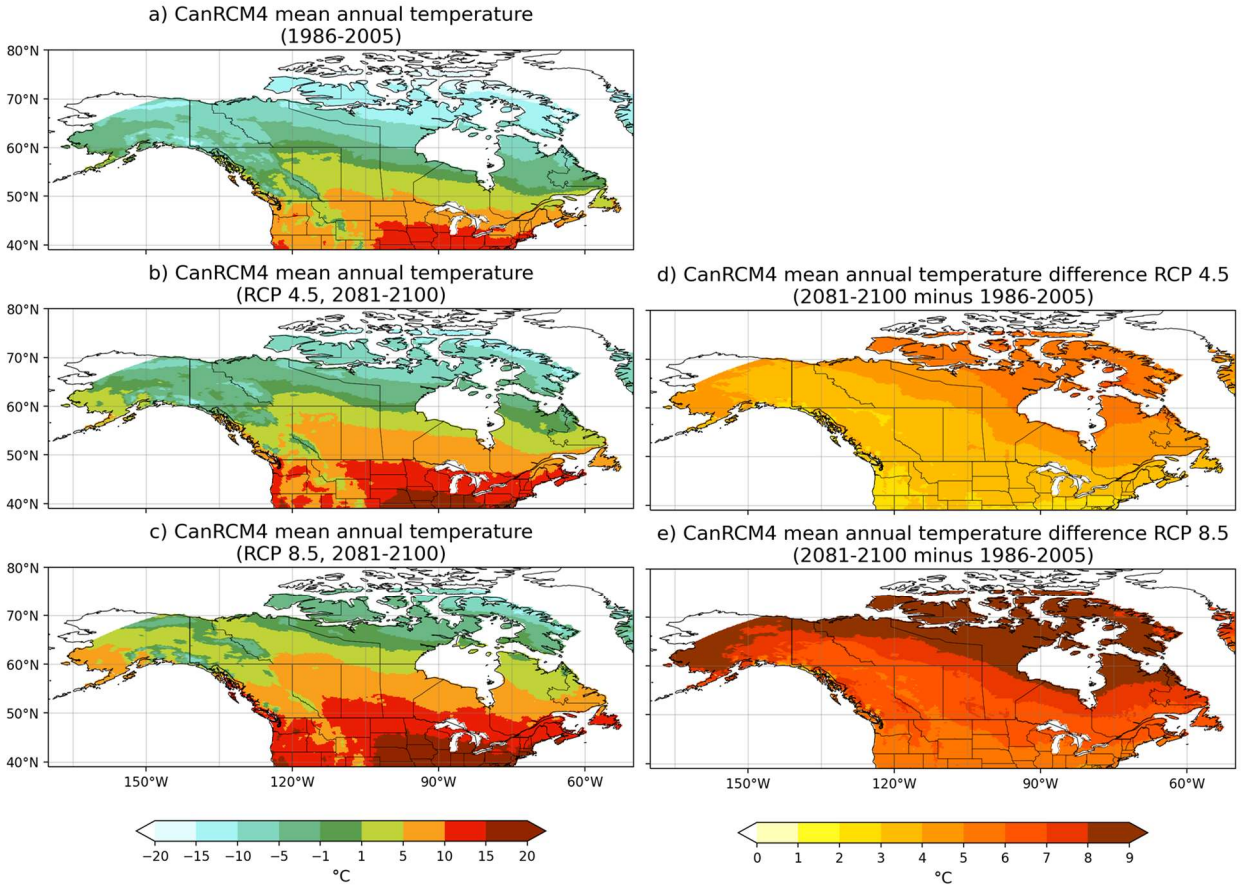

519 **Figure 6**: Comparison of CanRCM4 simulated temperature for the 1986-2005 period and for the
520 2081-2100 periods, for RCP 4.5 and 8.5 scenarios.

521

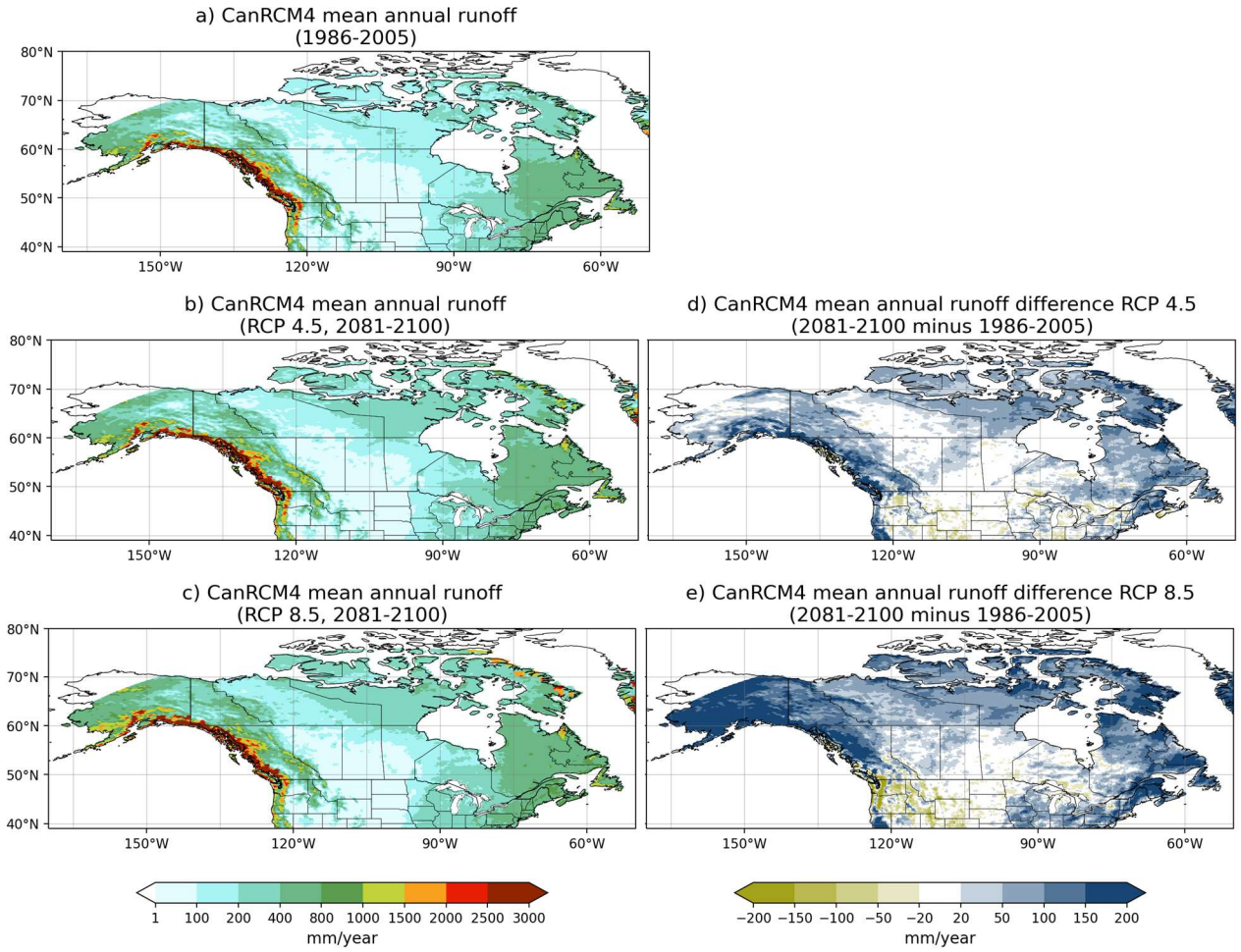

Figure 7: Comparison of CanRCM4 simulated runoff for the 1986-2005 period and the 2081-2100 periods, for RCP 4.5 and 8.5 scenarios.

In Figure 7 runoff increases generally everywhere in Canada for the RCP 4.5 and RCP 8.5 scenarios with larger changes on the west and east coasts, and in northern Canada, following a similar pattern of changes in precipitation. Runoff reduces in parts of the southern Columbia River basin in the United States in the RCP 4.5 scenario, and these decreases become more pronounced and widespread over the north-western Pacific region in the RCP 8.5 scenario including the Fraser River basin in Canada.

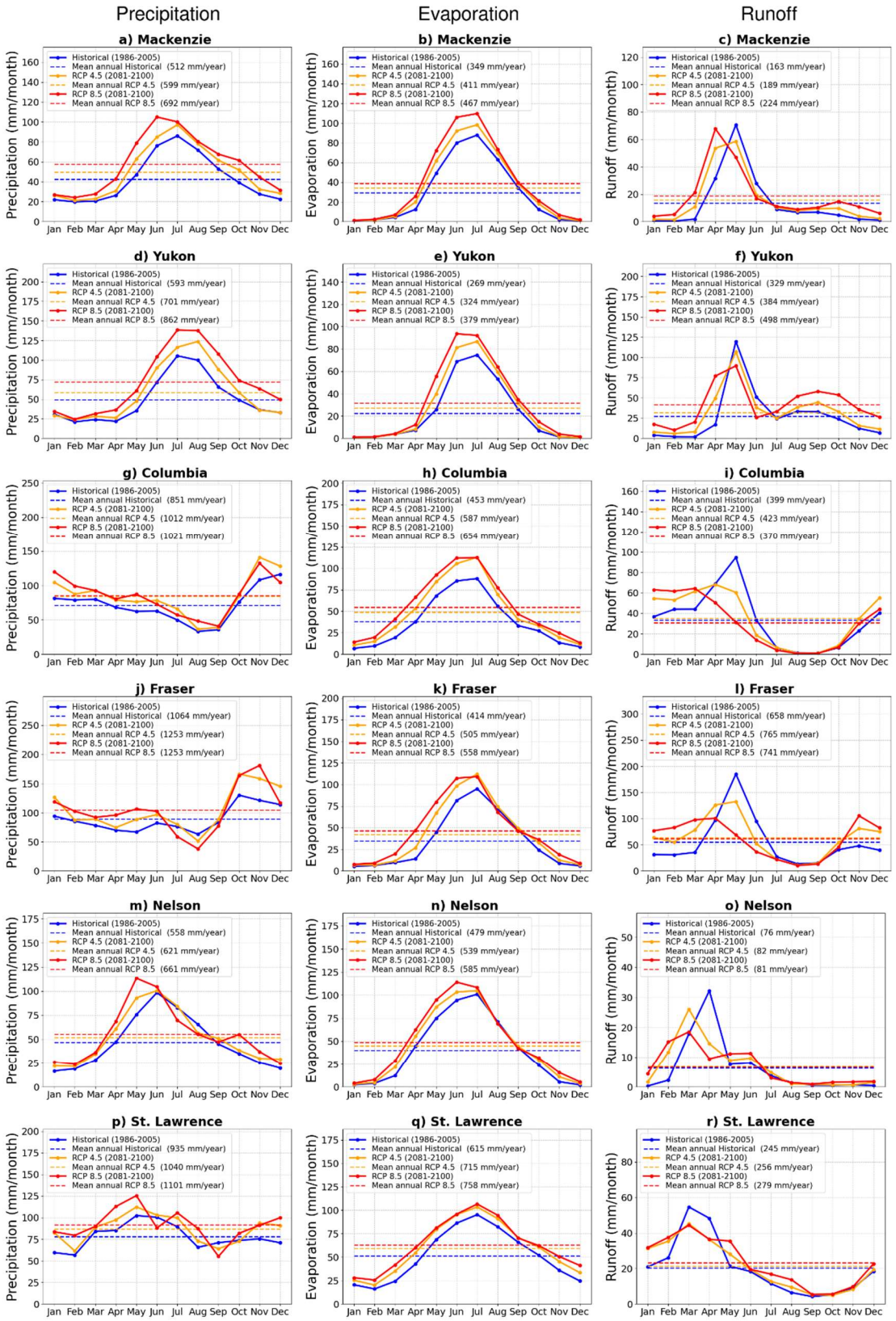

Figure 8: Comparison of the annual cycle of basin-wide averaged CanRCM4 simulated water budget components for each river basin for the historical (1986-2005) period and the two future scenarios RCP 4.5 and 8.5 (2081-2100): precipitation (left column), evaporation (middle column), and runoff (right column).

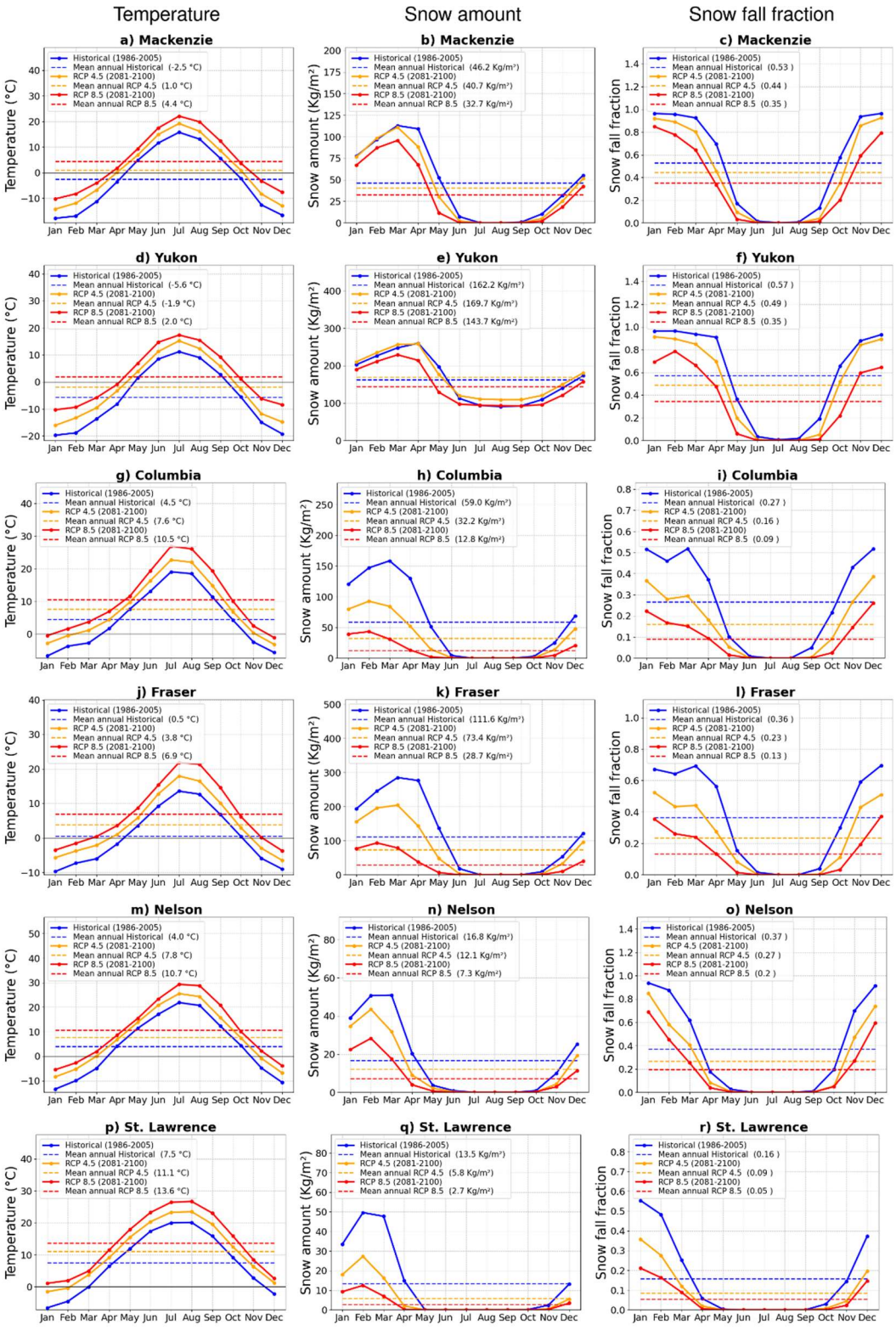

Figure 9: Comparison of the annual cycle of basin-wide averaged CanRCM4 simulated temperature (left column), snow water equivalent amount (middle column), and snowfall fraction (right column) for the historical (1986-2005) period and the two future scenarios RCP 4.5 and 8.5 (2081-2100).

609 Figure 8 shows the annual cycle of the simulated water budget components
610 (precipitation, evaporation, and runoff) for the six river basins considered in this study for the
611 historical (1986-2005) period and the two future scenarios, RCP 4.5 and 8.5 (2081-2100). As in
612 Figure 4, the mean annual values are shown as dashed lines, and their magnitude is noted in the
613 legend.

614 **Table 2**: Evaporation and runoff ratios for the six river basins simulated by CanRCM4 for the
615 historical period (1986-2005) and the two future scenarios (RCP 4.5 and 8.5, 2081-2100). The
616 evaporation (runoff) ratio is the ratio of mean annual evaporation (runoff) to precipitation.
617

River basin	Evaporation ratio (E/P)			Runoff ratio (R/P)		
	Historical (1986-2005)	RCP 4.5 (2081-2100)	RCP 8.5 (2081-2100)	Historical (1986-2005)	RCP 4.5 (2081-2100)	RCP 8.5 (2081-2100)
Mackenzie	0.682	0.686	0.675	0.318	0.316	0.324
Yukon	0.454	0.462	0.440	0.555	0.548	0.579
Columbia	0.532	0.580	0.641	0.469	0.418	0.362
Fraser	0.389	0.403	0.445	0.618	0.611	0.591
Nelson	0.858	0.868	0.885	0.136	0.132	0.123
St. Lawrence	0.664	0.686	0.684	0.314	0.294	0.302

618

619 The evaporation (E/P) and runoff (R/P) ratios for the six river basins for the historical period and
620 the two future scenarios are shown in Table 2 and allow to see how the partitioning of
621 precipitation into evaporation and runoff changes with climate. For the mean annual values of P,
622 E, and R reported in Figure 8, P is balanced to within 1% by E+R for all river basins (except St.
623 Lawrence) and all scenarios, except for the Yukon (for RCP 8.5) and Fraser River basins (for RCP
624 4.5 and 8.5) for which (E+R) is higher than P indicating that ΔS is not zero (see equation 1). As a
625 result, (E/P) and (R/P) also add to one for all river basins except for the Yukon (RCP
626 8.5,$(E+R)/P = 1.02$) and the Fraser River (RCP 4.5, $(E+R)/P = 1.014$, and RCP 8.5,
627 $(E+R)/P = 1.036$) basins. For the St. Lawrence River basin, the imbalance is around 2%
628 because of the presence of the Great Lakes which had to be excluded from the river basin mask.

629 Since basin-wide averaged calculations are done at 0.5° latitude-longitude resolution, and the
630 actual domain of CanRCM4 is on a rotated latitude-longitude projection this led to slightly more
631 rounding errors for the St. Lawrence than other river basins.

632 For all river basins considered, precipitation increases for both future scenarios with the
633 increase being larger for the RCP 8.5 scenario consistent with Figures 5d and 5e. The response of
634 evaporation to changes in climate is expected. The increase in precipitation and temperature
635 yields an increase in evaporation for future scenarios for all river basins. Simulated runoff does
636 not increase as much as precipitation since evaporation also increases. The runoff ratio, in Table
637 2, increases for the northerly Mackenzie and the Yukon River basins while it decreases for the
638 southerly Nelson, St. Lawrence, and especially for the Fraser and Columbia River basins which
639 are characterized by milder climate owing to their location in the Pacific north-western region.
640 This is because the increase in precipitation is more than enough to compensate for the increase
641 in evaporation (associated with a warmer climate) for the northern river basins but not for the
642 southern ones (as seen earlier in Figure 7 where runoff begins to decrease in parts of the
643 Columbia and Fraser River basins). The absolute runoff amount in Figure 8 increases for the
644 Mackenzie and Yukon River basins, in the RCP 4.5 and 8.5 scenarios compared to the historical
645 simulation, but doesn't change much for the Columbia, Fraser, Nelson, and St. Lawrence River
646 basins. However, the seasonality of runoff changes for all river basins, and the peak in simulated
647 runoff either occurs earlier in the year, occurs with reduced magnitude, or both. Canadian rivers
648 are dominated by spring snowmelt and this runoff behaviour is associated with snow melt
649 occurring earlier in the year in the RCP 4.5 scenario than in the historical simulation and occurring
650 even earlier in the RCP 8.5. This is seen in Figure 9 which shows the simulated annual cycle of

651 temperature changes, snow amount, and snowfall as a fraction of total precipitation for the
652 historical period and the two RCP scenarios for the six river basins. In Figure 9 the mean annual
653 temperature increases from the historical period to the RCP 4.5 scenario, and from the RCP 4.5
654 to RCP 8.5 scenario, are between 3 and 3.5 °C for the six river basins considered here. The middle
655 column of Figure 9 shows that in addition to earlier snowmelt the amount of snow in the winter
656 months decreases for all river basins with climate warming. The only exception to this is the
657 Yukon River basin in which the mean annual snow amount increases marginally in the RCP 4.5
658 scenario (Figure 9e). As expected, the fraction of precipitation falling as snow also decreases with
659 climate warming for all river basins (right column, Figure 9).

660

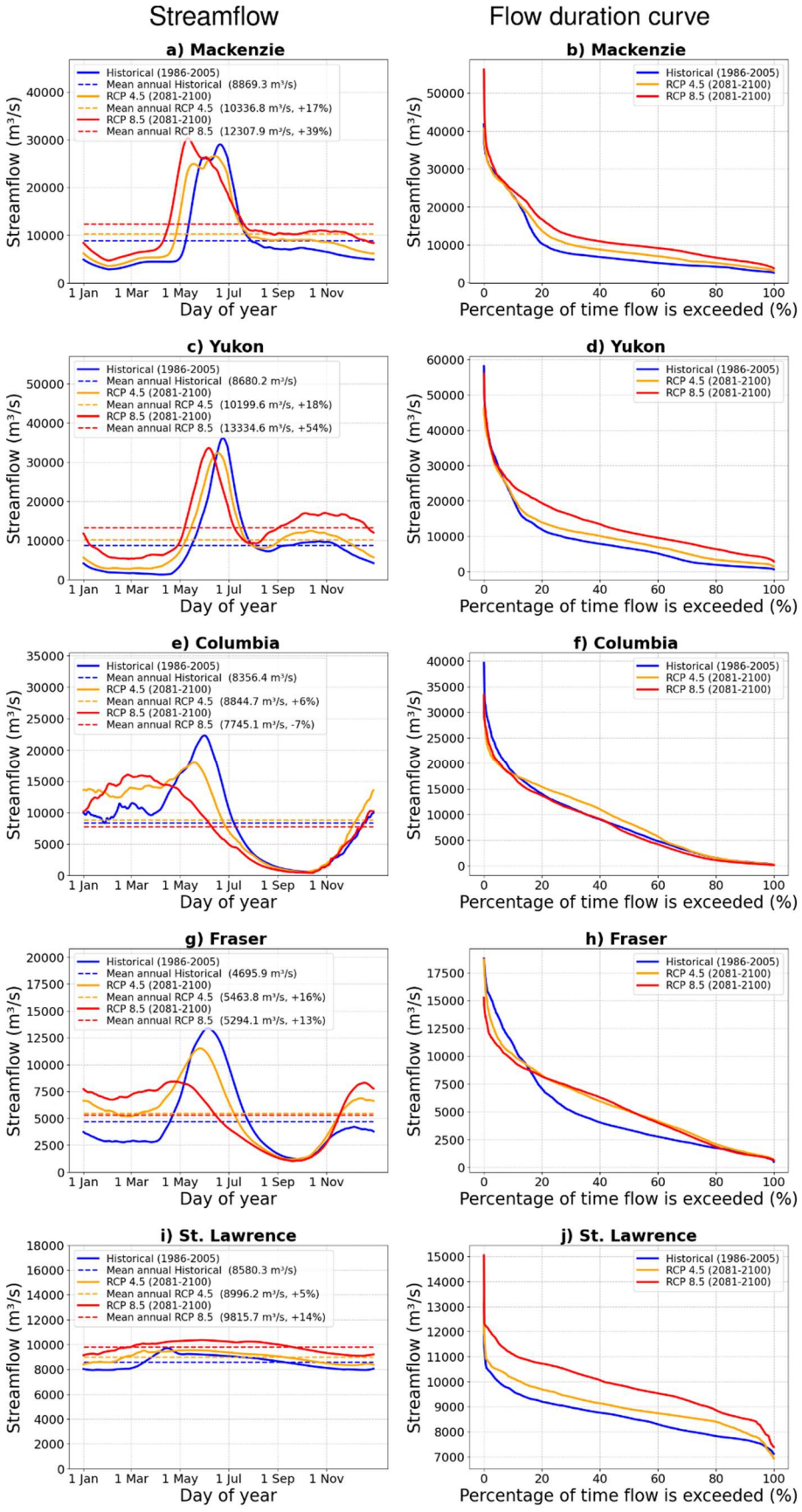

Figure 10: Comparison of the simulated daily streamflow (left column) and flow duration curves (right column) for the historical (1986-2005) period and the two future scenarios RCP 4.5 and 8.5 (2081-2100) for the river basins considered. The Nelson River is excluded for which we only evaluated annual streamflow values that are mentioned in the text.

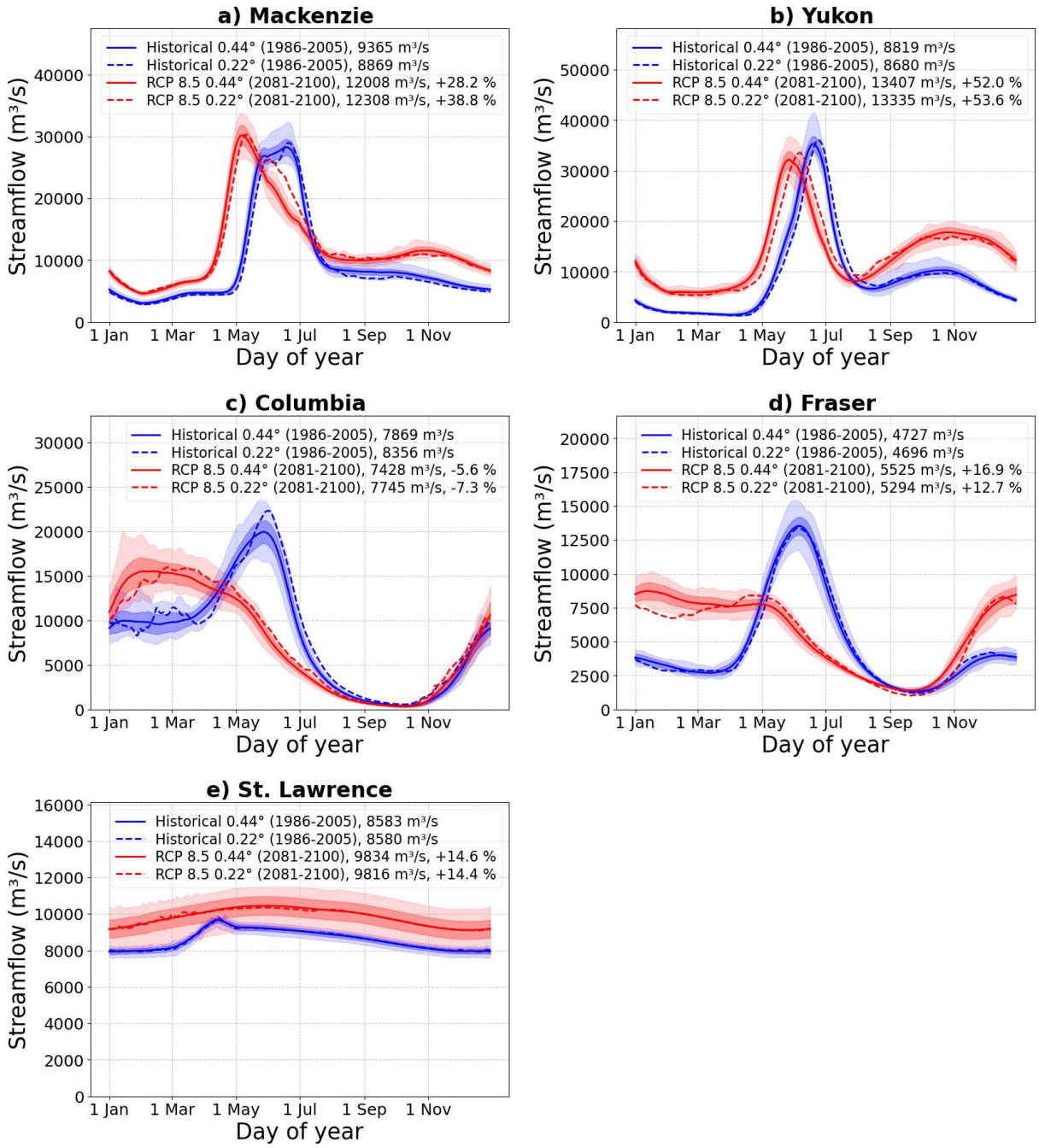

687 **Figure 11**: Comparison of the simulated daily streamflow for the historical (1986-2005) period
688 and the RCP 8.5 scenario (2081-2100) for the river basins considered in this study from the
689 0.22° and 0.44° simulations. The results from the 0.22° simulations (shown earlier in Figure 10)
690 are shown as dashed lines. The uncertainty range for the 0.44° simulations is based on results
691 from CanRCM4's 50-member large ensemble. The solid lines indicate the mean across 50
692 members the light shading indicates the full range, and the dark shading indicates the mean ±
693 one standard deviation range, for the 0.44° simulations. The Nelson River is excluded for which

694 only annual streamflow values are analyzed.
695
696 Figure 10 compares simulated daily streamflow and flow duration curves averaged over
697 the historical (1986-2005) period with those averaged over the two future scenarios RCP 4.5 and
698 8.5 (2081-2100) for the river basins considered here excluding the Nelson River. The flow
699 duration curves are calculated using daily streamflow values. The legends in Figure 10 for the
700 streamflow figures in the left column show mean annual values but also the change from the
701 simulated historical values for the RCP 4.5 and 8.5 scenarios. The mean annual streamflow
702 increases for all rivers for both the RCP 4.5 and 8.5 scenarios, except for the Columbia River for
703 the RCP 8.5 scenario (-7%). The increase in simulated annual streamflow is largest for the
704 Mackenzie (+16%, +39%) and Yukon Rivers (+17%, +53%) for the RCP 4.5 and 8.5 scenarios, due
705 to higher precipitation increase in these two basins (Figure 8). The increase in annual streamflow
706 for other rivers is smaller and between 6% and 14%. Daily streamflow and flow duration curves
707 are not shown for the Nelson River because we do not consider anthropogenic flow regulation,
708 as mentioned earlier. The simulated mean annual streamflow for the Nelson River increases from
709 2556.6 m^3/s (for the 1986-2005 period) to 2774.8 and 2723.8 m^3/s for the RCP 4.5 (+9%) and 8.5
710 (+7%) scenarios, respectively (for the period 2081-2100).

711 The changes in streamflow seasonality are larger for the southerly Columbia and Fraser
712 Rivers than for the northerly Mackenzie and Yukon Rivers. The peak daily streamflow for the
713 Yukon River still occurs in June given it's the coldest river basin (Figure 4d) and the streamflow
714 seasonality is still dominated by the spring snowmelt. The simulated daily peak streamflow for
715 the Yukon River occurs on 24 June for the historical period (1986-2005), and 18 June and 6 June,

716 respectively, for RCP 4.5 and 8.5 scenarios for the period 2081-2100. Streamflow for the Yukon
717 River also begins to increase earlier due to earlier snowmelt (Figure 9e). While the spring peak
718 streamflow reduces in both RCP 4.5 and 8.5 scenarios during June and part of July, streamflow
719 increases for most other months for the Yukon River. The Mackenzie River shows similar
720 behaviour to the Yukon River in terms of earlier shifts of spring streamflow peaks with climate
721 warming but the spring peak is higher for the RCP 8.5 scenario. The mean simulated daily peak
722 streamflow for the Mackenzie River occurs on 21 June for the historical period (1986-2005), and
723 14 June and 11 May, respectively, for RCP 4.5 and 8.5 scenarios for the period 2081-2100. Similar
724 to Yukon, although the streamflow is lower for the Mackenzie River during June and part of July,
725 it increases for most other months. The corresponding changes in streamflow are also seen in
726 the flow duration curves. For these two rivers the frequency of the occurrence of flows that occur
727 greater than about 5% of the time in the historical simulation increases in the future. The
728 Columbia and the Fraser Rivers experience much larger changes in their seasonality as their
729 primarily snow-dominated flow regimes change to more hybrid flow regimes. The snowmelt-
730 driven streamflow peak in spring is reduced considerably for future scenarios since a lower
731 fraction of fall, winter, and spring precipitation falls as snow. As a result, streamflow increases
732 from October to April since precipitation falling as rain, as opposed to snow, yields runoff that
733 runs straight into the rivers. Additionally, the large reduction in snowpack volume together with
734 earlier melt (Figure 9k and 9h) affects the seasonality of the Fraser and Columbia Rivers
735 streamflow and causes pronounced shifts in peak flows. The mean simulated daily peak
736 streamflow for the Columbia River occurs on 1 June for the historical period (1986-2005), and 19
737 May and 25 February, respectively, for RCP 4.5 and 8.5 scenario for the period 2081-2100. For

738 the Fraser River, the mean simulated peak streamflow occurs on 5 June for the historical period
739 (1986-2005), and 26 May and 21 April, respectively, for RCP 4.5 and 8.5 scenario for the period
740 2081-2100. The pronounced changes in the Fraser River basin peak flow are apparent in its flow
741 duration curve (Figure 10h) which shows a decrease (increase) in the frequency of streamflow
742 events which occurred less (more) than about 16% of the time and result in a more equitable
743 streamflow regime with a pronounced reduction in its seasonality. The simulated streamflow for
744 the St. Lawrence River shows very little seasonality and since annual streamflow increases for
745 both scenarios, the flow duration curve simply moves up (Figure 10j).

746 **3.3 Uncertainty in simulated changes in future streamflow**

747 Using the large ensemble simulations that are available for the historical period and the
748 RCP 8.5 scenario at 0.44 ° resolution we quantified the uncertainty in the simulated streamflow
749 associated with the internal variability of the CanRCM4 model. Similar to the 0.22° resolution,
750 we regridded the 0.44° runoff at CanRCM4's rotated latitude longitude projection to 0.5° regular
751 latitude longitude projection for use as input into the river routing scheme. This is illustrated in
752 Figure 11 which shows the simulated daily streamflow for all the rivers considered here except
753 the Nelson River. In Figure 11, the solid lines show the average across the 50 members of the
754 large ensemble, light shading shows the full range of the results, and dark shading shows the
755 mean ± one standard deviation range (this implies the 16%-84%, i.e. 68%, range when assuming
756 normally distributed monthly streamflow values). In addition, streamflow from the 0.22°
757 simulations (from Figure 10) is shown as dashed lines to allow direct comparison of results from
758 the 0.22° and 0.44° simulations.

The changes in simulated streamflow are consistent between the 0.22° and 0.44° simulations. The results from the 0.44° simulations are also notably smoother compared to the 0.22° simulations since the 0.44° results are also averaged over the 50 ensemble members in addition to the 20 years. For the most part, the results from the 0.22° simulations lie within the full range of results from the 0.44° simulations. This is expected since the driving climate at the boundaries of CanRCM4 based on CanESM2 is the same in both resolutions. The magnitude of change from the historical to the RCP 8.5 scenario (see legend for individual rivers) is, however, somewhat different. This is also expected because the coarser resolution 0.44° simulations are less representative of the basin topography than the 0.22°simulations. The day of peak streamflow occurs a few days earlier in 0.22° simulations than in the 0.44° simulations for the Mackenzie and Yukon Rivers. Overall, the large ensemble from the 0.44° simulations helps to provide context for results from the 0.22° simulations.

Overall, despite the differences in the magnitude of changes, the direction and variability of change obtained from this study is generally consistent with the previous studies using basin-scale hydrologic models, driven by statistically downscaled and bias-corrected climate model data, for instance for the Fraser River (Islam et al., 2019; Shrestha et al., 2012), the Columbia River (Schnorbus et al., 2014) and the Yukon River (Hay and McCabe, 2010). The results presented here are also comparable to the projections from global and regional scale hydrologic models, e.g. for the Mackenzie River basin (Krysanova et al., 2017, 2020).

4. Summary and conclusions

779 This study offers a consistent analysis of results across six river basins in Canada based on
780 results from the CanRCM4 model. Despite the biases in simulated present-day CanRCM4 climate,
781 and some differences in the results based on 0.22° and 0.44° simulations, the results provide
782 useful information about changes in simulated streamflow that is consistent with expectations
783 of process behaviour in a warmer climate, and with published studies.

784 Neither future precipitation nor temperature changes are uniform across Canada.
785 Simulated precipitation increases are higher closer to the west and east coasts, and simulated
786 temperature changes are higher towards the Arctic. Similar to precipitation, runoff changes are
787 also higher closer to the west and east coasts. The changes in simulated streamflow indicate how
788 the present-day climate state of river basins plays a role in their response to climate change. The
789 results yield two broadly distinct responses of monthly streamflow changes to climate warming,
790 up until the end of this century, for the northerly Mackenzie and Yukon rivers and the southerly
791 Fraser and Columbia rivers. Despite higher future projected temperature changes in Canada's
792 north, peak streamflow for the Mackenzie and Yukon rivers is still dominated by the spring
793 snowmelt. This is because the present-day colder states of these river basins imply that even
794 after around 6-7 °C warming, the basin-wide average temperatures are cold enough to not
795 sufficiently change their snowmelt-dominated streamflow regimes. Changes, however, do occur
796 in streamflow seasonality for these two rivers. Mean peak daily streamflow occurs earlier by
797 about 6-7 days for the Mackenzie and Yukon Rivers in the RCP 4.5 scenario and about 28 days for
798 the Mackenzie River and 12 days for the Yukon River for the RCP 8.5 scenario (Figure 10). The
799 earlier start of the snowmelt is the primary factor for the changes in peak streamflow and its time
800 of occurrence, while the streamflow increases during the rest of the year (except for June and

801 part of July) are driven by an increase in precipitation. Additionally, a higher fraction of winter
802 precipitation occurring as rainfall drives the winter streamflow increases. In contrast, the
803 streamflow seasonality for the southerly Fraser and Columbia rivers is significantly more affected
804 by warmer temperatures because the mean annual basin-wide temperature for these river basins
805 is already above 0° C for the historical period. Both these rivers experience pronounced changes
806 in their streamflow seasonality. The peak daily streamflow for both rivers decreases considerably
807 and occurs about 45 days earlier for the Fraser River and about 100 days earlier for the Columbia
808 River in the RCP 8.5 scenario. These results compare reasonably to the 1-2 months earlier peak
809 in previous studies for the Fraser River (Islam et al., 2019; Shrestha et al., 2012) but are higher
810 than the two months earlier peak for the Columbia River (Schnorbus et al., 2014) that used results
811 from multiple climate models. Shrestha et al. (2021a) used CanRCM4 data to evaluate snowpack
812 response to varying degrees of warming. They found that snowpack reduction using CanRCM4-
813 LE is higher than the ensemble of results obtained by driving a hydrological model with data from
814 other climate models (their supplementary information), consistent with CanESM2's higher
815 climate sensitivity. For the Nelson and the St. Lawrence Rivers which show very little seasonality
816 the effect of climate change is reflected in the changes in mean annual streamflow.

817 The results presented here also appear to show that the simulated changes in streamflow
818 are somewhat resolution-dependent. This would be expected especially for topography-
819 dominated river basins. If a large ensemble of 50 members for the 0.22° resolution was also
820 available, it would have been easier to draw firm conclusions about the effect of the spatial
821 resolution on changes in simulated streamflow.

There are two primary limitations of the work presented here. First, we use results from only one climate model. It would have been ideal to use runoff from other regional climate models to provide an uncertainty range based on the spread across different climate models. This would have also allowed us to evaluate how the spread across models compares to the spread across the 50 members of the CanRCM4 large ensemble. Second, the results are based on direct output from the CanRCM4 climate model and direct climate model output is biased. This limitation is tied to our methodology. The use of bias-corrected climate data inevitably implies using a different hydrological model or land surface scheme, than the land surface component of CanRCM4, and forcing it with bias-corrected climate data to obtain runoff. Finally, there are uncertainties associated with the routing process itself. As mentioned earlier, the routing scheme accounts for ice jams in a simplified manner, and anthropogenic flow regulation is not taken into account. The implicit assumption when using raw climate model output is that, despite the biases in simulated climate, it is possible to derive useful information about the impact of climate change on the simulated streamflow and other components of the hydrological budget. The Canada-wide results presented here have allowed us to differentiate between the hydrological response of the northerly Mackenzie and Yukon Rivers, and the southerly Fraser and Columbia Rivers, to climate change in a consistent manner. Furthermore, our results help fill the gaps in regions across Canada, where no climate model-driven hydrological projections are available. Within the scope of this study, we have only evaluated streamflow at the mouth of the six major rivers considered here. The full data set of daily simulated streamflow for the 20-year historical (1986-2005) and future periods (2081-2100) for the two scenarios, based on runoff from the 0.22° simulations, is made available as detailed in the data availability section.

Large ensembles are now becoming more common. The challenge for similar future studies is to consider the inter-model and intra-model (based on ensemble members of the same model) spreads in the same framework to derive an uncertainty estimate that takes into account both types of uncertainties.

Acknowledgment

We thank Daniel Peters for the helpful discussions at the beginning of this work and Sal Curasi and Gesa Meyer for providing comments on the final version of this manuscript. We also acknowledge the efforts of the climate modelling team at the Canadian Centre for Climate Modelling and Analysis (CCCma) who made the results from CanRCM4 available. We also thank the two anonymous reviewers who provided useful comments and helped us address the questions related to model bias and the differences in land surface and hydrological models. Finally, we would like to thank our handling editor (Alexander Gruber) for taking on our manuscript and giving us the opportunity to revise our manuscript.

Data availability

The CanRCM4 data from 0.22° simulations used in this study are available from CCCma website (https://climate-modelling.canada.ca/climatemodeldata/canrcm/CanRCM4/). The data from the 0.44° CanRCM4 large ensemble are available from Environment and Climate Change Canada (https://open.canada.ca/data/en/dataset/83aa1b18-6616-405e-9bce-af7ef8c2031c).

NetCDF files of simulated daily streamflow from the historical (1986-2005) and the two future scenarios (RCP 4.5 and 8.5, 2081-2100) at 0.5° resolution are available on Zenodo for the entire North American domain of CanRCM4 (doi:10.5281/zenodo.12775139, https://zenodo.org/records/12775139). These streamflow data correspond to the runoff from the 0.22° simulations.

Author contributions

VKA designed the study and wrote the majority of the manuscript. AL implemented river routing to operate at 0.5° resolution and performed all the simulations. RS and AL contributed to the manuscript text. RS also performed a literature review of existing studies that focus on

879 the impact of climate change on Canadian rivers.
880
881 **Competing interests**
882
883 The authors declare that they have no competing interests.
884

885 **References**

886 Alaya, M. A. B., Zwiers, F., and Zhang, X.: Evaluation and Comparison of CanRCM4 and CRCM5 to
887 Estimate Probable Maximum Precipitation over North America, J. Hydrometeorol., 20, 2069–2089,
888 https://doi.org/10.1175/JHM-D-18-0233.1, 2019.

889 Arora, V., Seglenieks, F., Kouwen, N., and Soulis, E.: Scaling aspects of river flow routing, Hydrol.
890 Process., 15, 461–477, https://doi.org/10.1002/hyp.161, 2001.

891 Arora, V. K. and Boer, G. J.: Effects of simulated climate change on the hydrology of major river basins, J.
892 Geophys. Res. Atmospheres, 106, 3335–3348, https://doi.org/10.1029/2000JD900620, 2001.

893 Arora, V. K. and Boer, G. J.: A Representation of Variable Root Distribution in Dynamic Vegetation
894 Models, Earth Interact., 7, 1–19, https://doi.org/10.1175/1087-3562(2003)007<0001:AROVRD>2.0.CO;2,
895 2003.

896 Arora, V. K. and Boer, G. J.: A parameterization of leaf phenology for the terrestrial ecosystem
897 component of climate models, Glob. Change Biol., 11, 39–59, https://doi.org/10.1111/j.1365-
898 2486.2004.00890.x, 2005.

899 Arora, V. K. and Boer, George. J.: A variable velocity flow routing algorithm for GCMs, J. Geophys. Res.
900 Atmospheres, 104, 30965–30979, https://doi.org/10.1029/1999JD900905, 1999.

901 Arora, V. K. and Harrison, S.: Upscaling river networks for use in climate models, Geophys. Res. Lett., 34,
902 https://doi.org/10.1029/2007GL031865, 2007.

903 Arora, V. K., Boer, G. J., Christian, J. R., Curry, C. L., Denman, K. L., Zahariev, K., Flato, G. M., Scinocca, J.
904 F., Merryfield, W. J., and Lee, W. G.: The Effect of Terrestrial Photosynthesis Down Regulation on the
905 Twentieth-Century Carbon Budget Simulated with the CCCma Earth System Model, J. Clim., 22, 6066–
906 6088, https://doi.org/10.1175/2009JCLI3037.1, 2009.

907 Arora, V. K., Scinocca, J. F., Boer, G. J., Christian, J. R., Denman, K. L., Flato, G. M., Kharin, V. V., Lee, W.
908 G., and Merryfield, W. J.: Carbon emission limits required to satisfy future representative concentration
909 pathways of greenhouse gases, Geophys. Res. Lett., 38, n/a-n/a,
910 https://doi.org/10.1029/2010GL046270, 2011.

911 Beltaos, S.: Advances in river ice hydrology, Hydrol. Process., 14, 1613–1625,
912 https://doi.org/10.1002/1099-1085(20000630)14:9<1613::AID-HYP73>3.0.CO;2-V, 2000.

913 Bonsal, B., Shrestha, R. R., Dibike, Y., Peters, D. L., Spence, C., Mudryk, L., and Yang, D.: Western
914 Canadian Freshwater Availability: Current and Future Vulnerabilities, Environ. Rev., 28, 528–545,
915 https://doi.org/10.1139/er-2020-0040, 2020.

916 Budhathoki, S., Rokaya, P., and Lindenschmidt, K.-E.: Impacts of future climate on the hydrology of a
917 transboundary river basin in northeastern North America, J. Hydrol., 605, 127317,
918 https://doi.org/10.1016/j.jhydrol.2021.127317, 2022.

919 Chegwidden, O. S., Nijssen, B., Rupp, D. E., Arnold, J. R., Clark, M. P., Hamman, J. J., Kao, S.-C., Mao, Y.,
920 Mizukami, N., Mote, P. W., Pan, M., Pytlak, E., and Xiao, M.: How Do Modeling Decisions Affect the
921 Spread Among Hydrologic Climate Change Projections? Exploring a Large Ensemble of Simulations
922 Across a Diversity of Hydroclimates, Earths Future, 7, 623–637, https://doi.org/10.1029/2018EF001047,
923 2019.

924 Chen, Y. and She, Y.: Long-term variations of river ice breakup timing across Canada and its response to
925 climate change, Cold Reg. Sci. Technol., 176, 103091,
926 https://doi.org/10.1016/j.coldregions.2020.103091, 2020.

927 Côté, J., Gravel, S., Méthot, A., Patoine, A., Roch, M., and Staniforth, A.: The Operational CMC–MRB
928 Global Environmental Multiscale (GEM) Model. Part I: Design Considerations and Formulation, Mon.
929 Weather Rev., 126, 1373–1395, https://doi.org/10.1175/1520-0493(1998)126<1373:TOCMGE>2.0.CO;2,
930 1998.

931 Deser, C., Lehner, F., Rodgers, K. B., Ault, T., Delworth, T. L., DiNezio, P. N., Fiore, A., Frankignoul, C.,
932 Fyfe, J. C., Horton, D. E., Kay, J. E., Knutti, R., Lovenduski, N. S., Marotzke, J., McKinnon, K. A., Minobe, S.,
933 Randerson, J., Screen, J. A., Simpson, I. R., and Ting, M.: Insights from Earth system model initial-
934 condition large ensembles and future prospects, Nat. Clim. Change, 10, 277–286,
935 https://doi.org/10.1038/s41558-020-0731-2, 2020.

936 Dibike, Y., Muhammad, A., Shrestha, R. R., Spence, C., Bonsal, B., de Rham, L., Rowley, J., Evenson, G.,
937 and Stadnyk, T.: Application of dynamic contributing area for modelling the hydrologic response of the
938 Assiniboine River basin to a changing climate, J. Gt. Lakes Res., 47, 663–676,
939 https://doi.org/10.1016/j.jglr.2020.10.010, 2021.

940 ECCC: The Canadian Regional Climate Model Large Ensemble. Environment and Climate Change Canada
941 (ECCC), Government of Canada Open Data Portal. Available at:
942 https://open.canada.ca/data/en/dataset/83aa1b18-6616-405e-9bce-af7ef8c2031c, Gatineau, QC,
943 Canada, 2018.

944 Gosling, S. N., Taylor, R. G., Arnell, N. W., and Todd, M. C.: A comparative analysis of projected impacts
945 of climate change on river runoff from global and catchment-scale hydrological models, Hydrol. Earth
946 Syst. Sci., 15, 279–294, https://doi.org/10.5194/hess-15-279-2011, 2011.

947 Harris, I., Osborn, T. J., Jones, P., and Lister, D.: Version 4 of the CRU TS monthly high-resolution gridded
948 multivariate climate dataset, Sci. Data, 7, 109, https://doi.org/10.1038/s41597-020-0453-3, 2020.

949 Hattermann, F. F., Vetter, T., Breuer, L., Su, B., Daggupati, P., Donnelly, C., Fekete, B., Flörke, F., Gosling,
950 S. N., P Hoffmann, Liersch, S., Masaki, Y., Motovilov, Y., Müller, C., Samaniego, L., Stacke, T., Wada, Y.,

951 Yang, T., and Krysnaova, V.: Sources of uncertainty in hydrological climate impact assessment: a cross-
952 scale study, Environ. Res. Lett., 13, 015006, https://doi.org/10.1088/1748-9326/aa9938, 2018.

953 Hay, L. E. and McCabe, G. J.: Hydrologic effects of climate change in the Yukon River Basin, Clim. Change,
954 100, 509–523, https://doi.org/10.1007/s10584-010-9805-x, 2010.

955 Hewitson, B. C., Daron, J., Crane, R. G., Zermoglio, M. F., and Jack, C.: Interrogating empirical-statistical
956 downscaling, Clim. Change, 122, 539–554, https://doi.org/10.1007/s10584-013-1021-z, 2014.

957 Huang, S., Shah, H., Naz, B. S., Shrestha, N., Mishra, V., Daggupati, P., Ghimire, U., and Vetter, T.: Impacts
958 of hydrological model calibration on projected hydrological changes under climate change—a multi-
959 model assessment in three large river basins, Clim. Change, 163, 1143–1164,
960 https://doi.org/10.1007/s10584-020-02872-6, 2020.

961 Hundecha, Y., Arheimer, B., Berg, P., Capell, R., Musuuza, J., Pechlivanidis, I., and Photiadou, C.: Effect of
962 model calibration strategy on climate projections of hydrological indicators at a continental scale, Clim.
963 Change, 163, 1287–1306, https://doi.org/10.1007/s10584-020-02874-4, 2020.

964 Islam, S. U., Curry, C. L., Déry, S. J., and Zwiers, F. W.: Quantifying projected changes in runoff variability
965 and flow regimes of the Fraser River Basin, British Columbia, Hydrol. Earth Syst. Sci., 23, 811–828,
966 https://doi.org/10.5194/hess-23-811-2019, 2019.

967 Ismail, H., Rowshon, M. K., Hin, L. S., Abdullah, A. F. B., and Nasidi, N. M.: Assessment of climate change
968 impact on future streamflow at Bernam river basin Malaysia, IOP Conf. Ser. Earth Environ. Sci., 540,
969 012040, https://doi.org/10.1088/1755-1315/540/1/012040, 2020.

970 Kourzeneva, E., Asensio, H., Martin, E., and Faroux, S.: Global gridded dataset of lake coverage and lake
971 depth for use in numerical weather prediction and climate modelling, Tellus Dyn. Meteorol. Oceanogr.,
972 https://doi.org/10.3402/tellusa.v64i0.15640, 2012.

973 Krysanova, V., Vetter, T., Eisner, S., Huang, S., Pechlivanidis, I., Michael Strauch, Gelfan, A., Kumar, R.,
974 Aich, V., Arheimer, B., Chamorro, A., Griensven, A. van, Kundu, D., Lobanova, A., Mishra, V., Plötner, S.,
975 Reinhardt, J., Ousmane Seidou, Wang, X., Wortmann, M., Zeng, X., and Hattermann, F. F.:
976 Intercomparison of regional-scale hydrological models and climate change impacts projected for 12
977 large river basins worldwide—a synthesis, Environ. Res. Lett., 12, 105002, https://doi.org/10.1088/1748-
978 9326/aa8359, 2017.

979 Krysanova, V., Zaherpour, J., Didovets, I., Gosling, S. N., Gerten, D., Hanasaki, N., Müller Schmied, H.,
980 Pokhrel, Y., Satoh, Y., Tang, Q., and Wada, Y.: How evaluation of global hydrological models can help to
981 improve credibility of river discharge projections under climate change, Clim. Change, 163, 1353–1377,
982 https://doi.org/10.1007/s10584-020-02840-0, 2020.

983 L. Sushama, R. Laprise, D. Caya, A. Frigon, and M. Slivitzky: Canadian RCM projected climate-change
984 signal and its sensitivity to model errors, Int J Clim., 26, 2141–2159, 2006.

985 Lange, S.: Trend-preserving bias adjustment and statistical downscaling with ISIMIP3BASD (v1. 0),
986 Geosci. Model Dev., 12, 2019.

MacDonald, M. K., Stadnyk, T. A., Déry, S. J., Braun, M., Gustafsson, D., Isberg, K., and Arheimer, B.: Impacts of 1.5 and 2.0 °C Warming on Pan-Arctic River Discharge Into the Hudson Bay Complex Through 2070, Geophys. Res. Lett., 45, 7561–7570, https://doi.org/10.1029/2018GL079147, 2018.

Manning, R.: On the flow of water in open channels and pipes, Trans. Inst. Civ. Eng. Irel., XX, 161–207, 1891.

Maraun, D.: Bias Correcting Climate Change Simulations - a Critical Review, Curr. Clim. Change Rep., 2, 211–220, https://doi.org/10.1007/s40641-016-0050-x, 2016.

Maraun, D., Shepherd, T. G., Widmann, M., Zappa, G., Walton, D., Gutiérrez, J. M., Hagemann, S., Richter, I., Soares, P. M. M., Hall, A., and Mearns, L. O.: Towards process-informed bias correction of climate change simulations, Nat. Clim. Change, 7, 764–773, https://doi.org/10.1038/nclimate3418, 2017.

Miller, J. R. and Russell, G. L.: The impact of global warming on river runoff, J. Geophys. Res. Atmospheres, 97, 2757–2764, https://doi.org/10.1029/91JD01700, 1992.

Miller, O. L., Putman, A. L., Alder, J., Miller, M., Jones, D. K., and Wise, D. R.: Changing climate drives future streamflow declines and challenges in meeting water demand across the southwestern United States, J. Hydrol. X, 11, 100074, https://doi.org/10.1016/j.hydroa.2021.100074, 2021.

Moss, R. H., Edmonds, J. A., Hibbard, K. A., Manning, M. R., Rose, S. K., van Vuuren, D. P., Carter, T. R., Emori, S., Kainuma, M., Kram, T., Meehl, G. A., Mitchell, J. F. B., Nakicenovic, N., Riahi, K., Smith, S. J., Stouffer, R. J., Thomson, A. M., Weyant, J. P., and Wilbanks, T. J.: The next generation of scenarios for climate change research and assessment, Nature, 463, 747–756, https://doi.org/10.1038/nature08823, 2010.

Oki, T. and Sud, Y. C.: Design of Total Runoff Integrating Pathways (TRIP)—A Global River Channel Network, Earth Interact., 2, 1–37, https://doi.org/10.1175/1087-3562(1998)002<0001:DOTRIP>2.3.CO;2, 1998.

Poitras, V., Sushama, L., Seglenieks, F., Khaliq, M. N., and Soulis, E.: Projected Changes to Streamflow Characteristics over Western Canada as Simulated by the Canadian RCM, J. Hydrometeorol., 12, 1395–1413, https://doi.org/10.1175/JHM-D-10-05002.1, 2011.

Prowse, T. D.: Ice jam characteristics, Liard–Mackenzie rivers confluence, Can. J. Civ. Eng., 13, 653–665, https://doi.org/10.1139/l86-100, 1986.

Quinn, F. H.: Hydraulic Residence Times for the Laurentian Great Lakes, J. Gt. Lakes Res., 18, 22–28, https://doi.org/10.1016/S0380-1330(92)71271-4, 1992.

Salathé, E. P., Leung, L. R., Qian, Y., and Zhang, Y.: Regional climate model projections for the State of Washington, Clim. Change, 102, 51–75, https://doi.org/10.1007/s10584-010-9849-y, 2010.

von Salzen, K., Scinocca, J. F., McFarlane, N. A., Li, J., Cole, J. N. S., Plummer, D., Verseghy, D., Reader, M. C., Ma, X., Lazare, M., and Solheim, L.: The Canadian Fourth Generation Atmospheric Global Climate Model (CanAM4). Part I: Representation of Physical Processes, Atmosphere-Ocean, 51, 104–125, https://doi.org/10.1080/07055900.2012.755610, 2013.

Schlund, M., Lauer, A., Gentine, P., Sherwood, S. C., and Eyring, V.: Emergent constraints on equilibrium climate sensitivity in CMIP5: do they hold for CMIP6?, Earth Syst. Dyn., 11, 1233–1258, https://doi.org/10.5194/esd-11-1233-2020, 2020.

Schnorbus, M., Werner, A., and Bennett, K.: Impacts of climate change in three hydrologic regimes in British Columbia, Canada, Hydrol. Process., 28, 1170–1189, https://doi.org/10.1002/hyp.9661, 2014.

Scinocca, J. F., Kharin, V. V., Jiao, Y., Qian, M. W., Lazare, M., Solheim, L., Flato, G. M., Biner, S., Desgagne, M., and Dugas, B.: Coordinated Global and Regional Climate Modeling, J. Clim., 29, 17–35, https://doi.org/10.1175/JCLI-D-15-0161.1, 2016.

Shi, H., Li, T., and Wei, J.: Evaluation of the gridded CRU TS precipitation dataset with the point raingauge records over the Three-River Headwaters Region, J. Hydrol., 548, 322–332, https://doi.org/10.1016/j.jhydrol.2017.03.017, 2017.

Shrestha, R. R., Schnorbus, M. A., Werner, A. T., and Berland, A. J.: Modelling spatial and temporal variability of hydrologic impacts of climate change in the Fraser River basin, British Columbia, Canada, Hydrol. Process., 26, 1840–1860, https://doi.org/10.1002/hyp.9283, 2012.

Shrestha, R. R., Cannon, A. J., Schnorbus, M. A., and Alford, H.: Climatic Controls on Future Hydrologic Changes in a Subarctic River Basin in Canada, J. Hydrometeorol., 20, 1757–1778, https://doi.org/10.1175/JHM-D-18-0262.1, 2019.

Shrestha, R. R., Bonsal, B. R., Bonnyman, J. M., Cannon, A. J., and Najafi, M. R.: Heterogeneous snowpack response and snow drought occurrence across river basins of northwestern North America under 1.0°C to 4.0°C global warming, Clim. Change, 164, 40, https://doi.org/10.1007/s10584-021-02968-7, 2021a.

Shrestha, R. R., Bonsal, B. R., Kayastha, A., Dibike, Y. B., and Spence, C.: Snowpack response in the Assiniboine-Red River basin associated with projected global warming of 1.0 °C to 3.0 °C, J. Gt. Lakes Res., 47, 677–689, https://doi.org/10.1016/j.jglr.2020.04.009, 2021b.

Sobie, S. R. and Murdock, T. Q.: Projections of Snow Water Equivalent Using a Process-Based Energy Balance Snow Model in Southwestern British Columbia, J. Appl. Meteorol. Climatol., 61, 77–95, https://doi.org/10.1175/JAMC-D-20-0260.1, 2022.

Stadnyk, T. A., Tefs, A., Broesky, M., Déry, S. J., Myers, P. G., Ridenour, N. A., Koenig, K., Vonderbank, L., and Gustafsson, D.: Changing freshwater contributions to the Arctic: A 90-year trend analysis (1981–2070), Elem. Sci. Anthr., 9, https://doi.org/10.1525/elementa.2020.00098, 2021.

Sun, Q., Miao, C., Duan, Q., Ashouri, H., Sorooshian, S., and Hsu, K.-L.: A Review of Global Precipitation Data Sets: Data Sources, Estimation, and Intercomparisons, Rev. Geophys., 56, 79–107, https://doi.org/10.1002/2017RG000574, 2018.

Swart, N. C., Cole, J. N. S., Kharin, V. V., Lazare, M., Scinocca, J. F., Gillett, N. P., Anstey, J., Arora, V., Christian, J. R., Hanna, S., Jiao, Y., Lee, W. G., Majaess, F., Saenko, O. A., Seiler, C., Seinen, C., Shao, A., Sigmond, M., Solheim, L., von Salzen, K., Yang, D., and Winter, B.: The Canadian Earth System Model version 5 (CanESM5.0.3), Geosci. Model Dev., 12, 4823–4873, https://doi.org/10.5194/gmd-12-4823-2019, 2019.

Thrasher, B., Xiong, J., Wang, W., Melton, F., Michaelis, A., and Nemani, R.: Downscaled Climate Projections Suitable for Resource Management, Eos Trans. Am. Geophys. Union, 94, 321–323, https://doi.org/10.1002/2013EO370002, 2013.

Trenberth, K. E., Smith, L., Qian, T., Dai, A., and Fasullo, J.: Estimates of the Global Water Budget and Its Annual Cycle Using Observational and Model Data, J. Hydrometeorol., 8, 758–769, https://doi.org/10.1175/JHM600.1, 2007.

Verseghy, D. L.: Class—A Canadian land surface scheme for GCMS. I. Soil model, Int. J. Climatol., 11, 111–133, https://doi.org/10.1002/joc.3370110202, 1991.

Verseghy, D. L., McFarlane, N. A., and Lazare, M.: Class—A Canadian land surface scheme for GCMS, II. Vegetation model and coupled runs, Int. J. Climatol., 13, 347–370, https://doi.org/10.1002/joc.3370130402, 1993.

Werner, A. T., Schnorbus, M. A., Shrestha, R. R., Cannon, A. J., Zwiers, F. W., Dayon, G., and Anslow, F.: A long-term, temporally consistent, gridded daily meteorological dataset for northwestern North America, Sci. Data, 6, 180299, https://doi.org/10.1038/sdata.2018.299, 2019.

Winter, J. M. and Eltahir, E. A. B.: Modeling the hydroclimatology of the midwestern United States. Part 2: future climate, Clim. Dyn., 38, 595–611, https://doi.org/10.1007/s00382-011-1183-1, 2012.

Wong, J. S., Razavi, S., Bonsal, B. R., Wheater, H. S., and Asong, Z. E.: Inter-comparison of daily precipitation products for large-scale hydro-climatic applications over Canada, Hydrol. Earth Syst. Sci., 21, 2163–2185, https://doi.org/10.5194/hess-21-2163-2017, 2017.

Yoosefdoost, I., Khashei-Siuki, A., Tabari, H., and Mohammadrezapour, O.: Runoff Simulation Under Future Climate Change Conditions: Performance Comparison of Data-Mining Algorithms and Conceptual Models, Water Resour. Manag., 36, 1191–1215, https://doi.org/10.1007/s11269-022-03068-6, 2022.

Zhang, X., Tang, Q., Zhang, X., and Lettenmaier, D. P.: Runoff sensitivity to global mean temperature change in the CMIP5 Models, Geophys. Res. Lett., 41, 5492–5498, https://doi.org/10.1002/2014GL060382, 2014.